NASA
Technical Memorandum 106878

Army Research Laboratory
Technical Report ARL–TR–722

# Minimization of the Vibration Energy of Thin-Plate Structures and the Application to the Reduction of Gearbox Vibration

Katsumi Inoue
*Lewis Research Center*
*Cleveland, Ohio*

and

Timothy L. Krantz
*Vehicle Propulsion Directorate*
*U.S. Army Research Laboratory*
*Lewis Research Center*
*Cleveland, Ohio*

December 1995

National Aeronautics and
Space Administration



U.S. ARMY
RESEARCH LABORATORY

# MINIMIZATION OF THE VIBRATION ENERGY OF THIN-PLATE STRUCTURES AND THE APPLICATION TO THE REDUCTION OF GEARBOX VIBRATION

Katsumi Inoue[1]
Tohoku University
Sendai, Japan

and

Timothy L. Krantz
Vehicle Propulsion Directorate
U.S. Army Research Laboratory
Lewis Research Center
Cleveland, Ohio 44135

## SUMMARY

While the vibration analysis of gear systems has been developed, a systematic approach to the reduction of gearbox vibration has been lacking. The technique of reducing vibration by shifting natural frequencies is proposed here for gearboxes and other thin-plate structures using the theories of finite elements, modal analysis, and optimization. A triangular shell element with 18 degrees of freedom is developed for structural and dynamic analysis. To optimize, the overall vibration energy is adopted as the objective function to be minimized at the excitation frequency by varying the design variable (element thickness) under the constraint of overall constant weight. Modal analysis is used to determine the sensitivity of the vibration energy as a function of the eigenvalues and eigenvectors. The optimum design is found by the gradient projection method and a unidimensional search procedure. By applying the computer code to design problems for beams and plates, it was verified that the proposed method is effective in reducing vibration energy. The computer code is also applied to redesign the NASA Lewis gear noise rig test gearbox housing. As one example, only the shape of the top plate is varied, and the vibration energy levels of all the surfaces are reduced, yielding an overall reduction of 1/5 compared to the initial design. As a second example, the shapes of the top and two side plates are varied to yield an overall reduction in vibration energy of 1/30.

## INTRODUCTION

The users of geared power transmissions desire lightweight, low-cost systems with high efficiency, large power capacity, longevity, and low vibration and noise. Recently, the reduction of noise caused by gears seems to be of growing importance, as end users perceive products with low noise and vibration to be of overall high quality. A project team was organized at the NASA Lewis Research Center to reduce transmission noise in helicopter cabins.

Most vibration energy of a gear system is generated at the gear mesh. The vibration energy is then transmitted to the gearbox housing through the shafts and bearings where the energy causes housing vibration and so-called structure-borne noise. To estimate the vibration and noise of a gear system, the exciting source of the gear mesh and the dynamic behavior of the system must be considered. Once the vibration of a gearbox is determined by analysis or measurement (refs. 1 to 5), the sound radiated from the gearbox can be calculated by applying principles of acoustics (ref. 6).

In spite of the progress made toward estimating and analyzing gearbox noise, more knowledge is necessary to establish methods of gearbox noise reduction. For example, an effective method of vibration reduction used for many products is to shift the natural frequencies of vibration to avoid resonance by adding a mass or stiffener at a strategic location. However, the method is not easily employed, as it is difficult to foresee the proper location for the mass or stiffener and then estimate the shift of the natural frequency. Recently, much progress was made in optimization procedures (refs. 7 to 10), and their use is becoming more common and valuable. With these ideas in

[1]National Research Council (NRC) Research Associate at the NASA Lewis Research Center.

mind, research was conducted to develop a method of reducing transmission noise by designing the housing for low vibration via structural optimization. The focus of this work was to design the gearbox housing for minimum vibration for a given level of excitation at the gear mesh. Of course, controlling the excitation source by proper design of the gear mesh is also important.

A method was developed to reduce the housing vibration via the finite-element method coupled with modal analysis and optimization techniques. First, a self-contained and compact, yet flexible, finite element computer program was developed for the analysis of thin-plate and shell structures. The finite element used was a three-node triangular element with 18 degrees of freedom. Second, modal analysis theory was applied, and the eigenvalue problem was solved. Third, an optimization technique was introduced to the analysis procedure.

In this work, the overall vibration energy was selected as the objective function to be minimized by optimization. In many cases, the dynamic response or transfer function is used as an index of vibration. For example, the mobility, which is the velocity caused by a unit-exciting force, could be used as the objective function. However, the mobility indicates the response only at the selected point. Here, the overall vibration energy was selected as the index of vibration and was used as the objective function for this application. The thicknesses of the elements were selected as the design variables, and the technique of modal analysis was used to derive vibration energy sensitivity with respect to the design variables. Optimum values for the element thickness were then computed by a gradient project method (ref. 11) with a unidimensional search procedure under the constraint condition of constant weight for the structure.

This report describes the theory of the methods, the computer program (REVISE) based on these theories, and its application to some sample problems involving beams, plates, and gearbox housing. The computations are all based on unit harmonic forces. The frequency responses, vibration energies, and optimum shapes are calculated and illustrated. Finally, results and conclusions from the sample problems are discussed concerning the newly developed noise reduction method and its application to gearbox noise reduction.

## SYMBOLS

| | |
|---|---|
| a | shape function coefficient |
| A | element area |
| b | shape function coefficient |
| c | shape function coefficient |
| [C] | damping matrix |
| {d} | steepest descent vector |
| D | flexural rigidity |
| E | Young's elastic modulus |
| f | frequency |
| {f(t)} | exciting force vector |
| {F} | modal exciting force vector |
| g | behavior constraint |
| h | side constraint |
| [I] | unit matrix |
| k | stiffness |
| [K] | stiffness matrix |
| L | shape function |
| (m,n) | mode shape |
| [M] | mass matrix |
| N | shape function |
| *N* | degrees of freedom |
| P | load |
| [P] | projection matrix |
| [Q] | coefficient matrix |

| | |
|---|---|
| s | step size |
| t | thickness |
| T | vibration energy |
| [T] | coordinate transformation matrix |
| u | displacement; displacement in x direction |
| $\{u(t)\}$ | displacement vector |
| $\{\dot{u}(t)\}$ | velocity vector |
| $\{\ddot{u}(t)\}$ | acceleration vector |
| U | work done per unit load |
| $U^*$ | work done by element unit strain |
| $\{U\}$ | complex amplitude vector |
| v | displacement in y direction |
| w | displacement in z direction |
| $w^R$ | rigid body motion displacement |
| $w^*$ | element strain displacement |
| W | weight of structure |
| $\overline{W}$ | prescribed weight of structure |
| $\{x\}$ | design variable |
| $\{y\}$ | undamped eigenvector |
| X, Y, Z | Cartesian coordinates |
| $\{z\}$ | damped eigenvector |
| $\alpha$ | proportional damping factor for mass |
| $\beta$ | proportional damping factor for stiffness |
| $\delta_{rs}$ | Kronecker's delta |
| $\{\delta\}$ | nodal displacement vector |
| $\{\delta^*\}$ | relative nodal displacement vector |
| $\theta$ | element rotation |
| $\lambda$ | undamped eigenvalue |
| $[\lambda]$ | diagonal matrix of eigenvalues |
| $[\Lambda]$ | coordinate transformation matrix |
| $\mu$ | damped eigenvalue |
| $\nu$ | Poisson's ratio |
| $\{\xi(t)\}$ | modal coordinate displacement vector |
| $\{\dot{\xi}(t)\}$ | modal coordinate velocity vector |
| $\rho$ | mass density |
| $\{\phi\}$ | normalized eigenvector |
| $[\Phi]$ | modal matrix |
| $\omega$ | undamped natural angular frequency |

Subscripts

| | |
|---|---|
| B | submatrix |
| ex | excitation |
| n | number of modes considered |
| o | initial |
| q | number of constraint surfaces |
| r | counter for order of eigenvector |

| | |
|---|---|
| rI | imaginary part of r-th component |
| rR | real part of r-th component |
| s | counter for order of eigenvector |

Superscripts

| | |
|---|---|
| e | element |
| k | k-th iteration |
| T | transpose of matrix or vector |

## THEORETICAL FUNDAMENTALS

### Modal Analysis of Forced Vibration

Vibration analysis of linear systems based on the mode shapes of natural vibration is commonly called modal analysis. The main purpose for applying modal analysis here is to convert a set of simultaneous differential equations into a set of independent differential equations by linear transformation of coordinates. Let an elastic structure be discretized into finite elements with *N* degrees of freedom. The equation of motion can then be given in matrix form as

$$[M]\{\ddot{u}(t)\}+[C]\{\dot{u}(t)\}+[K]\{u(t)\}=\{f(t)\} \tag{1}$$

where [M] is the mass matrix, [C] is the damping matrix, [K] is the stiffness matrix, {u(t)} is the displacement vector, and {f(t)} is the exciting force vector. By assuming proportional damping, the damping matrix may be represented by a linear combination of the mass matrix and stiffness matrix as

$$[C]=\alpha[M]+\beta[K] \tag{2}$$

The eigenvalue problem that is related to equation (1) for the case of proportional damping can be described as

$$\mu^2[M]\{z\}+\mu(\alpha[M]+\beta[K])\{z\}+[K]\{z\}=\{0\} \tag{3}$$

The eigenvalue $\mu$ and the eigenvector {z} in equation (3) are obtained from

$$\lambda=-\frac{(\mu^2+\alpha\mu)}{(\beta\mu+1)}$$
$$\{z\}=\{y\} \tag{4}$$

where $\lambda$ and {y} are the eigenvalue and eigenvector of the undamped vibration system with the same matrices [M] and [K] such that

$$[K]\{y\}=\lambda[M]\{y\} \tag{5}$$

If matrices [M] and [K] are positive definite, as is usual for vibration systems, then $\lambda$, {y}, $\mu$, and {z} are real and the eigenvector {z} has the orthogonal properties

$$\{z_r\}^T[M]\{z_r\} = m_r, \qquad \{z_r\}^T[M]\{z_s\} = 0 \qquad (r \neq s)$$

$$\{z_r\}^T[K]\{z_r\} = k_r, \qquad \{z_r\}^T[K]\{z_s\} = 0 \qquad (r \neq s) \tag{6}$$

$$\{z_r\}^T[C]\{z_r\} = c_r = \alpha m_r + \beta k_r, \qquad \{z_r\}^T[C]\{z_s\} = 0 \qquad (r \neq s)$$

In equation (6), subscripts r and s indicate the order of the eigenvectors. By ignoring modes of vibration beyond the frequency range of interest, we can reduce the degrees of freedom to be solved (i.e., r, s = 1 ... n ($n << N$)), where n eigenvectors are considered in the analysis. The related eigenvalues are given by

$$\lambda_r = \omega_r^2 = \frac{k_r}{m_r} \tag{7}$$

where $\omega_r$ is the r-th undamped natural angular frequency. By applying equation (6), the set of $N$ simultaneous equations that describes the motions of the system (eq. (1)) can be transformed and reduced into n independent differential equations.

In the particular case of harmonic vibration, the transformation mentioned above can be done more simply. Let $\{\phi\}$ be the eigenvector which is normalized with respect to mass matrix,

$$\{\phi_r\}^T[M]\{\phi_s\} = \delta_{rs} \tag{8}$$

where $\delta_{rs}$ is the Kronecker's delta. The modal matrix, $[\Phi]$, is defined by the assembly of these eigenvectors as

$$[\Phi] = \left[\{\phi_1\}, \{\phi_2\}, \ldots, \{\phi_n\}\right] \tag{9}$$

From equations (8) and (9), and applying the principle of Rayleigh's quotient, the following relation is derived instead of equation (6)

$$[\Phi]^T[M][\Phi] = [I]$$

$$[\Phi]^T[K][\Phi] = [\lambda] \tag{10}$$

In equation (10), [I] is an n×n unit matrix and $[\lambda]$ denotes the diagonal matrix composed of n eigenvalues. By the orthogonal properties of the modal coordinates, any displacement $\{u(t)\}$ can be approximately represented by a linear combination of the eigenvectors

$$\{u(t)\} = \sum_{r=1}^{n} \xi_r(t)\{\phi_r\} = [\Phi]\{\xi(t)\} \tag{11}$$

When the structure is excited by a harmonic force of angular frequency $\omega$, then the force can be described by

$$\{f(t)\} = \{F\}e^{j\omega t} \tag{12}$$

and the steady-state vibration of the structure can be written in the same form as

$$\{u(t)\} = \{U\}e^{j\omega t} = [\Phi]\{\xi\}e^{j\omega t} \tag{13}$$

Note that here, {U} is independent of time. Substituting equations (12) and (13) in equation (l) and pre-multiplying by $[\Phi]^T$ gives

$$-\omega^2[\Phi]^T[M][\Phi]\{\xi\}e^{j\omega t} + j\omega[\Phi]^T[C][\Phi]\{\xi\}e^{j\omega t} + [\Phi]^T[K][\Phi]\{\xi\}e^{j\omega t} = [\Phi]^T\{F\}e^{j\omega t} \tag{14}$$

By applying equation (10) to equation (14), n independent algebraic equations are obtained for the evaluation of the vector $\{\xi\}$ in matrix form as

$$-\omega^2\{\xi\} + j\omega\left[\alpha[I] + \beta[\lambda]\right]\{\xi\} + [\lambda]\{\xi\} = [\Phi]^T\{F\} \tag{15}$$

The r-th component is given by

$$\xi_r = \frac{\{\phi_r\}^T\{F\}}{\left[\left(\lambda_r - \omega^2\right) + j\omega\left(\alpha + \beta\lambda_r\right)\right]} \tag{16}$$

where r = 1, ..., n. Consequently, the complex amplitude {U} of the forced-vibration problem is obtained by substituting $\{\xi\}$ into equation (13).

## Vibration Energy and its Sensitivity

The velocity $\{\dot{u}(t)\}$ is generally represented in the same way as the displacement (eq.(11)) as

$$\{\dot{u}(t)\} = [\Phi]\{\dot{\xi}(t)\} \tag{17}$$

In case of harmonic excitation, from equation (17) the velocity can be written in the same form as equation (13),

$$\{\dot{u}(t)\} = \{\dot{U}\}e^{j\omega t} = [\Phi]\{\dot{\xi}\}e^{j\omega t} \tag{18}$$

The velocity can be directly derived by differentiating the displacement equation (13), directly giving

$$\{\dot{u}(t)\} = j\omega[\Phi]\{\xi\}e^{j\omega t} \tag{19}$$

From equations (18) and (19), the vector $\{\dot{\xi}\}$ is given by

$$\{\dot{\xi}\} = j\omega\{\xi\} \tag{20}$$

Therefore, the real and imaginary parts of the r-th component is obtained as follows

$$\dot{\xi}_{rR} = \frac{(\alpha + \beta\lambda_r)\{\phi_r\}^T\{F\}}{\left[\frac{1}{\omega^2}\left(\lambda_r - \omega^2\right)^2 + (\alpha + \beta\lambda_r)^2\right]}$$

$$\dot{\xi}_{rI} = \frac{\frac{1}{\omega}\left(\lambda_r - \omega^2\right)\{\phi_r\}^T\{F\}}{\left[\frac{1}{\omega^2}\left(\lambda_r - \omega^2\right)^2 + (\alpha + \beta\lambda_r)^2\right]} \tag{21}$$

The vibration energy T of the structure is given by

$$T = \frac{\left\{\dot{U}^*\right\}^T[M]\left\{\dot{U}\right\}}{2}$$

$$= \frac{\left\{\dot{\xi}^*\right\}^T[\Phi]^T[M][\Phi]\left\{\dot{\xi}\right\}}{2} \tag{22}$$

$$= \frac{\left\{\dot{\xi}^*\right\}^T\left\{\ddot{\xi}\right\}}{2}$$

where * indicates the conjugate complex; therefore, the energy is represented by

$$T = \frac{1}{2}\sum_{r=1}^{n}\left(\dot{\xi}_{rR}^2 + \dot{\xi}_{rI}^2\right) \tag{23}$$

The sensitivity of the vibration energy with respect to the design variable $x_i$ (i = 1, . . ., m) is obtained from

$$\frac{\partial T}{\partial x_i} = \sum_{r=1}^{n}\left(\dot{\xi}_{rR}\frac{\partial \dot{\xi}_{rR}}{\partial x_i} + \dot{\xi}_{rI}\frac{\partial \dot{\xi}_{rI}}{\partial x_i}\right) \tag{24}$$

The partial derivative terms of equation (24) can be determined from differentiating equation (21) by the design variables. Since $\alpha$, $\beta$, $\omega$, and $\{F\}$ are independent of the design variables, the sensitivity of the vibration energy can be found once the functions that describe the sensitivities of the eigenvalues and the eigenvectors are known. An explanation of their derivation follows.

## Sensitivities of Eigenvalue and Eigenvector

The derivation of the sensitivities of the eigenvalues and eigenvectors, summarized briefly in this section, is based on the method proposed by Fox (ref. 12).

The r-th (r = 1, ..., n) order eigenvalue $\lambda_r$ and eigenvector $\{\phi_r\}$ are obtained from the following equation:

$$[K]\{\phi_r\} = \lambda_r[M]\{\phi_r\} \tag{25}$$

Differentiating equation (25) by the design variable yields

$$\frac{\partial \lambda_r}{\partial x_i}[M]\{\phi_r\} = \left(\left[\frac{\partial K}{\partial x_i}\right] - \lambda_r\left[\frac{\partial M}{\partial x_i}\right]\right)\{\phi_r\} + \left([K] - \lambda_r[M]\right)\left\{\frac{\partial \phi_r}{\partial x_i}\right\} \tag{26}$$

Premultiplying equation (26) by $\{\phi_r\}^T\{\lambda_r\}^T$, the second term on the right-hand side vanishes because

$$\{\phi_r\}^T\left([K] - \lambda_r[M]\right) = \left[\left([K] - \lambda_r[M]\right)\{\phi_r\}\right]^T = 0 \tag{27}$$

Therefore, the sensitivity of the eigenvalue is given by

$$\frac{\partial \lambda_r}{\partial x_i} = \{\phi_r\}^T\left(\left[\frac{\partial K}{\partial x_i}\right] - \lambda_r\left[\frac{\partial M}{\partial x_i}\right]\right)\{\phi_r\} \tag{28}$$

Although equation (26) includes the sensitivity of the eigenvector, it can not be solved as written because the determinant of the sensitivity's coefficient matrix is equal to zero. So, an equation is introduced independently by differentiating the first relation of equation (10) to give

$$\{\phi_r\}^T[M]\frac{\partial \phi_r}{\partial x_i} = -\frac{1}{2}\{\phi_r\}^T\left[\frac{\partial M}{\partial x_i}\right]\{\phi_r\} \tag{29}$$

An appropriate row of matrix equation (26) is replaced by equation (29) to avoid a zero determinant. Then, the sensitivity of the eigenvector is calculated by solving the simultaneous equations. The row that relates to the largest eigenvector should be replaced to obtain the best solution.

## Search for the Optimum Value

The optimum design problem for this analysis is expressed as follows:

$$\begin{array}{ll} \text{Minimize} & T\{x\} \\ \text{Behavior constraint} & g\{x\} = \overline{W} - W\{x\} = 0 \\ \text{Side constraint} & h_1\{x\} = x_i - x_{min} \geq 0, \\ & h_2\{x\} = x_{max} - x_i \geq 0 \\ \text{Design variables} & \{x\} = \left(x_1, x_2, \ldots, x_N\right)^T \end{array} \tag{30}$$

The elements' thicknesses are the design variables $\{x\}$. The prescribed weight and the weight of the structure are represented by $\overline{W}$ and $W\{x\}$, respectively. By the behavior constraint, the designs are of constant total weight. Minimum and maximum limits are set for the elements' thickness by the side constraints, $h_1$ and $h_2$.

Many procedures search for the optimum value for this kind of problem by first obtaining the feasible direction along which the design variables are modified to minimize the objective function. In this analysis, the gradient projection method (ref. 11) (which can be applied to problems with linear or nonlinear constraints) is used to find

this direction. Following immediately is an outline of the procedure for the case of linear constraints as it applies to this research.

In the feasible region, the point corresponding to the current design is moved in the direction of the steepest descent vector $\{d^{(k)}\}$, and a new design is obtained by

$$\left\{x^{(k+1)}\right\} = \left\{x^{(k)}\right\} + s\left\{d^{(k)}\right\} \tag{31}$$

where

$$\left\{d^{(k)}\right\} = -\left\{\frac{\partial T\left(\left\{x^{(k)}\right\}\right)}{\partial x}\right\}$$

In this equation, the superscript (k) means the k-th iteration, and s is the step determined by a unidimensional search. When the new point $\{x^c\} = \{x^{(k+1)}\}$ reaches the intersection formed by the constraint surfaces, the steepest descent vector is projected to the intersection to obtain the next feasible direction. The projection of the descent vector is given by the following relations:

$$\left\{d^P\right\} = [P]\left\{d\left\{x^c\right\}\right\}$$

where

$$\begin{aligned}
[P] &= [I] - \{U\}[V]\{U\}^T \\
[V] &= \left[\{U\}^T\{U\}\right]^{-1} \\
\{U\} &= \left[\{u_1\}, \{u_2\}, \ldots, \{u_q\}\right] \\
\{u_i\} &= \left(\frac{\partial g_i}{\partial x_1}, \frac{\partial g_i}{\partial x_2}, \ldots, \frac{\partial g_i}{\partial x_N}\right)^T
\end{aligned} \tag{32}$$

To simplify, the constraint functions $g(\{x\})$, $h_1(\{x\})$, and $h_2(\{x\})$ are written as $g_i$ in equation (32). The matrix [P] is called the projection matrix. In a problem with linear constraints, the constraint surfaces are all planes. Therefore, the point obtained from equation (31) by using the projected vector $\{d^P\}$ always stays in the feasible region.

The steepest descent vector $\{d^{(k)}\}$ is formed by the sensitivity or the first derivative of the objective function as shown in equation (31). If the second derivative was obtained, the step in equation (31) could be evaluated by a faster method (e.g., the Newton-Raphson method). However, this would require the evaluation of the second derivatives of the eigenvalues and eigenvectors, which is fairly complicated. Therefore, the step is evaluated by the simple procedure explained below. Since the design variables in the current design $\{x^{(k)}\}$ are known, the value of the objective function can be evaluated. Let $T_1$ be the value, where the subscript 1 means the current design. Similarly, let $T_2^{(i)}$ and $T_3^{(i)}$ be the values of the objective function at the different states of design variables of the i-th iteration. The procedure can be itemized as follows:

(1) Estimate $T_1$
(2) Set $T_2^{(1)} = T_1$, $T_3^{(1)} = T_1$
(3) Assume the step $s^{(1)}$
(4) Evaluate $T_s^{(1)}$ by using $s^{(1)}$ and equations (31) and (32), if necessary
(5) Compare $T_s^{(1)}$ to $T_2^{(1)}$
(6) If $T_s^{(1)} > T_2^{(1)}$
then set $T_3^{(2)} = T_s^{(1)}$, $s^{(2)} = s^{(1)} / 2$
evaluate $T_s^{(2)}$ for $T_2^{(2)}$
return to (5) and continue until $T_s^{(i)} < T_2^{(i-1)}$

(7) If $T_s^{(1)} < T_2^{(1)}$
then set $T_2^{(2)} = T_s^{(1)}$, $s^{(2)} = 2 \times s^{(1)}$
evaluate $T_s^{(2)}$ for $T_3^{(2)}$
return to (5) and continue until $T_s^{(i)} > T_2^{(i)}$

This procedure finds the closed region $[\{x^{(k)}\}, \{x^{(k)}\} + s^{(i)}\{d^P\}]$ or $[\{x^{(k)}\}, \{x^{(k)}\} + 2s^{(i)}\{d^P\}]$, which contains the relative minimum. The lower and higher limits of the region give the value $T_1$ and $T_3^{(i)}$, and the middle point give the value $T_2^{(i)}$. If the region is found, the objective function is approximated locally by a quadratic expression based on these values, and the step that gives the minimum point of the quadratic expression can be determined. The procedure is ineffective for finding the region when the objective function decreases monotonously. In such a case, the procedure is stopped after the appropriate iterations and the step at the last iteration is taken as the solution. The value of the energy in the last iteration is stored and used for the judgment of convergence. The judging criteria for convergence is 1/1000th relative variation.

## OPTIMUM PROGRAM DESIGN

### Finite-Element Formulation

The best way to model the free surface of three-dimensional structures (e.g., a gearbox) for use with an optimization procedure may be to use triangular shell elements. Many kinds of elements have been proposed and successfully applied to both static and dynamic analyses. If the total degrees of freedom is constant, using a small number of high-precision elements generally leads to good results. However, a larger number of nodes is needed to describe the three-dimensional geometry of gearbox housing. Consequently, since the total degrees of freedom for the analysis must be practical, a three-node triangular element of 18 degrees of freedom was selected. The element matrices of the shell element were formulated by combining the matrices of plate bending and plane analysis problems (ref. 13). The formulation is summarized as follows:

Finite Element for Plate Bending.—The actual displacement of middle surface w (fig. 1) is represented by the sum of the deflection of the supported element $w^*$, which induces the strain in the element, and the displacement, $w^R$, caused by rigid body motion,

$$w = w^* + w^R \tag{33}$$

Using area coordinates, where i = 1, 2, 3,

$$\begin{aligned} L_i &= \frac{(a_i + b_i x + c_i y)}{A} \\ a_i &= x_{i+1}y_{i+2} - x_{i+2}y_{i+1} \\ b_i &= y_{i+1} - y_{i+2} \\ c_i &= x_{i+2} - x_{i+1} \\ A &= a_1 + a_2 + a_3 \end{aligned} \tag{34}$$

The displacement caused by rigid body motion is expressed as

$$w^R = \sum_{i=1}^{3} L_i w_i \tag{35}$$

where $w_i$ denotes the displacement at node i. In equation (34), if the subscript i+1 or i+2 is larger than 3, it represents the value subtracted by 3. The relative displacement at node i is defined by the rotations about the x and y axes,

$$\left\{\delta_i^*\right\}^e = \left(\theta_x^*, \theta_y^*\right)_i^T = \left(\frac{\partial w^x}{\partial y}, -\frac{\partial w^x}{\partial x}\right)_i^T = \left(\theta_x - \frac{\partial w^R}{\partial y}, \theta_y + \frac{\partial w^R}{\partial x}\right)_i^T \tag{36}$$

The relation between the relative nodal displacement $\{\delta^*\}^e$ and the actual nodal displacement $\{\delta\}^e$ is given by

$$\left\{\delta^*\right\}^e = [T]\{\delta\}^e \tag{37}$$

The matrix [T] is slightly different from the one given in reference 13 because of a difference in the definition of the nodal displacement in equation (36). The deflection $w^*$ is represented by

$$\begin{aligned} w^* &= \left[N_1, N_2, N_3\right]\left(\delta_1^*, \delta_2^*, \delta_3^*\right)^T \\ &= \sum_{i=1}^{3}\left(N_i^x\theta_{x_i}^* + N_i^y\theta_{y_i}^*\right) \end{aligned} \tag{38}$$

and the relative shape functions $N_i^y$ and $N_i^x$ are defined as follows:

$$\begin{aligned} N_i^x &= b_{i+1}\left(L_{i+2}L_i^2 + \frac{1}{2}L_iL_{i+1}L_{i+2}\right) - b_{i+2}\left(L_{i+1}L_i^2 + \frac{1}{2}L_iL_{i+1}L_{i+2}\right) \\ N_i^y &= c_{i+1}\left(L_{i+2}L_i^2 + \frac{1}{2}L_iL_{i+1}L_{i+2}\right) - c_{i+2}\left(L_{i+1}L_i^2 + \frac{1}{2}L_iL_{i+1}L_{i+2}\right) \end{aligned} \tag{39}$$

The element stiffness matrix is evaluated by

$$\left[K_B\right]^e = [T]^T\left[K_B^*\right]^e[T] \tag{40}$$

The (i,j) submatrix of $[K^*_B]$ is given by

$$\left[K^*_{B_{ij}}\right] = \int\int D\left[k^*\right]dx\,dy$$

$$\begin{aligned}
k_{11}^* &= \frac{\partial^2 N_i^x}{\partial xx}\frac{\partial^2 N_j^x}{\partial xx} + \nu\left(\frac{\partial^2 N_i^x}{\partial xx}\frac{\partial^2 N_j^x}{\partial yy} + \frac{\partial^2 N_i^x}{\partial yy}\frac{\partial^2 N_j^x}{\partial xx}\right) + \frac{\partial^2 N_i^x}{\partial yy}\frac{\partial^2 N_j^x}{\partial yy} + 2(1-\nu)\frac{\partial^2 N_i^x}{\partial xy}\frac{\partial^2 N_j^x}{\partial xy} \\
k_{12}^* &= \frac{\partial^2 N_i^x}{\partial xx}\frac{\partial^2 N_j^y}{\partial xx} + \nu\left(\frac{\partial^2 N_i^x}{\partial xx}\frac{\partial N_j^y}{\partial yy} + \frac{\partial^2 N_i^x}{\partial yy}\frac{\partial^2 N_j^y}{\partial xx}\right) + \frac{\partial^2 N_i^x}{\partial yy}\frac{\partial^2 N_j^y}{\partial yy} + 2(1-\nu)\frac{\partial^2 N_i^x}{\partial xy}\frac{\partial^2 N_j^y}{\partial xy} \\
k_{21}^* &= \frac{\partial^2 N_i^y}{\partial xx}\frac{\partial^2 N_j^x}{\partial xx} + \nu\left(\frac{\partial^2 N_i^y}{\partial xx}\frac{\partial N_j^x}{\partial yy} + \frac{\partial^2 N_i^y}{\partial yy}\frac{\partial^2 N_j^x}{\partial xx}\right) + \frac{\partial^2 N_i^y}{\partial yy}\frac{\partial^2 N_j^x}{\partial yy} + 2(1-\nu)\frac{\partial^2 N_i^y}{\partial xy}\frac{\partial^2 N_j^x}{\partial xy} \\
k_{22}^* &= \frac{\partial^2 N_i^y}{\partial xx}\frac{\partial^2 N_j^y}{\partial xx} + \nu\left(\frac{\partial^2 N_i^y}{\partial xx}\frac{\partial^2 N_j^y}{\partial yy} + \frac{\partial^2 N_i^y}{\partial yy}\frac{\partial^2 N_j}{\partial xx}\right) + \frac{\partial^2 N_i^y}{\partial yy}\frac{\partial^2 N_j^y}{\partial yy} + 2(1-\nu)\frac{\partial^2 N_i^y}{\partial xy}\frac{\partial^2 N_j^y}{\partial xy}
\end{aligned} \tag{41}$$

Here, D denotes the flexural rigidity of the plate. Every term in equation (41) is calculated by substituting equation (34) into equation (39) and then differentiating by x and y. For example, $\partial^2 N_i^x/\partial_{xx}$ is given by

$$\frac{\partial^2 N_i^x}{\partial xx} = \frac{1}{A^2}(b_{i+1} - b_{i+2})b_{i+1}b_{i+2}L_i$$

$$+\frac{1}{A^2}\left\{-2b_i^2 b_{i+2} + (b_{i+1} - b_{i+2})b_{i+2}b_i\right\}L_{i+1} \tag{42}$$

$$+\frac{1}{A^2}\left\{2b_i^2 b_{i+1} + (b_{i+1} - b_{i+2})b_i b_{i+1}\right\}L_{i+2}$$

The integration in equation (41) includes the combination of the integration of $L_iL_j$, where i,j = 1, 2, 3, and has the form

$$\iint L_iL_j dx\, dy = \frac{1}{A}\left\{\frac{1}{2}a_i a_j + \frac{1}{24}b_i b_j\left(x_1^2 + x_2^2 + x_3^2\right)\right.$$

$$\left.+\frac{1}{24}\left(b_i c_j + b_j c_i\right)\left(x_1y_1 + x_2y_2 + x_3y_3\right) + \frac{1}{24}c_i c_j\left(y_1^2 + y_2^2 + y_3^2\right)\right\} \tag{43}$$

The displacement w is rewritten in matrix form as

$$w = \left(\tilde{N}\right)\left\{\tilde{\delta}\right\}^e$$

$$\left(\tilde{N}\right) = \left(L_1, N_1^x, N_1^y, L_2, N_2^x, N_2^y, L_3, N_3^x, N_3^y\right) \tag{44}$$

$$\left\{\tilde{\delta}\right\} = \left(w_1, \theta_{x1}^*, \theta_{y1}^*, w_2, \theta_{x2}^*, \theta_{y2}^*, w_3, \theta_{x3}^*, \theta_{y3}^*\right)^T$$

The relationship between $\{\tilde{\delta}\}^e$ and $\{\delta\}^e$ is written in the same form as equation (37):

$$\left\{\tilde{\delta}\right\}^e = \left[\tilde{T}\right]\{\delta\}^e \tag{45}$$

The matrix $[\tilde{T}]$ of equation (45) has a dimension of 9×9. Substituting equation (45) into equation (44), we obtain

$$w = (N)\{\delta\}^e$$

$$(N) = \left(\tilde{N}\right)\left[\tilde{T}\right] = (L)[Q] \tag{46}$$

$$(L) = \left(L_1, L_2, L_3, L_1L_2^2, L_2L_3^2, L_3L_1^2, L_1^2L_2, L_2^2L_3, L_3^2L_1, L_1L_2L_3\right)$$

where matrix [Q] is the coefficient of (L) and has dimensions of 10×9. The consistent mass matrix $[M_B]^e$ is finally evaluated by the method of numeric integration

$$\left[M_B\right]^e = \iint \rho t(N)^T(N)\,dx\,dy = \rho t[Q]^T\left[\iint (L)^T(L)\,dx\,dy\right][Q] \tag{47}$$

where ρ and t are the mass density and element thickness, respectively.

Finite Element for Plane Analysis Problems.—The shape function for the plane analysis problem is given by

$$N_i = \frac{(a_i + b_i x + c_i y)}{A} \tag{48}$$

The consistent mass matrix $[M_p]^e$ is evaluated by the equation

$$\left[M_p\right]^e = \int\int \rho t (N)^T (N)\, dx\, dy$$

$$[N] = (N_1[I], N_2[I], N_3[I]) \tag{49}$$

where [I] is a 2×2 unit matrix. The (i,j) submatrix of the stiffness matrix $[K_p]^e$ is written

$$\left[K_{p_{ij}}\right] = \left(\frac{t}{2A}\right)\left(\frac{E}{1-\nu^2}\right)\begin{bmatrix} b_i b_j + \frac{1-\nu}{2} c_i c_j & \nu b_i c_j + \frac{1-\nu}{2} c_i b_j \\ \nu c_i b_j + \frac{1-\nu}{2} b_i c_j & c_i c_j + \frac{1-\nu}{2} b_i b_j \end{bmatrix} \tag{50}$$

The Shell Finite Element.—The nodal displacement is defined by the following expression, where i=1, 2, 3

$$\{\delta_i\} = \left(u,\ v,\ w,\ \theta_x,\ \theta_y, \theta_z\right)_i^T \tag{51}$$

Here, u, v, and w are displacements along x, y, and z axes while $\theta_x$, $\theta_y$, and $\theta_z$ are the rotations around x, y, and z axes.

The stiffness matrix for the shell element is obtained by combining the stiffness matrices of the plate-bending and plane analysis problems; therefore, the (i,j) submatrix has the form

$$\left[K_{ij}\right]^e = \begin{bmatrix} \left[K_{p_{ij}}\right] & 0 & 0 \\ 0 & \left[K_{B_{ij}}\right] & 0 \\ 0 & 0 & K_{\theta_z} \end{bmatrix} \tag{52}$$

In equation (52), $\{K_{\theta_z}\}$ indicates the stiffness for rotation about the axis normal to the element. However, it is difficult to formulate theoretically. The stiffness term $\{K_{\theta_z}\}$ is given approximately by the following matrix as was used in the present work:

$$\left\{K_{\theta_z}\right\} = \alpha \frac{EtA}{2} \begin{bmatrix} 1 & -0.5 & -0.5 \\ -0.5 & 1 & -0.5 \\ -0.5 & -0.5 & 1 \end{bmatrix} \begin{Bmatrix} \theta_{z1} \\ \theta_{z2} \\ \theta_{z3} \end{Bmatrix} \tag{53}$$

where $\alpha = 0.03$.

The mass matrix of the shell element can be formulated in the same way as the stiffness matrix. The transformation of the element stiffness matrix to the global coordinate system is defined in the ordinary way,

$$[K]^e_{global} = [\Lambda]^T [K]^e_{local} [\Lambda] \tag{54}$$

where the 18×18 matrix [Λ] is formed by putting the 3×3 direction cosine matrix in the diagonal submatrix.

## Structure of Computer Program REVISE

The computer code REVISE (REduction of VIbration in Structural Engineering) was developed following the procedures described in the previous sections and its structure is shown in figure 2. The program consists of two main parts. The first part is the analyzer, which is composed of the finite-element analysis, the eigenvalue analysis, and the evaluation of the vibration energy. The second part is the optimizer, which includes the sensitivity analysis and the search procedure for the optimum value. Two IMSL (ref. 14) routines are used to calculate simultaneous equations and invert matrices. The user can control the flow of the computations by input parameters and may obtain the result of the eigenvalue analysis only. This control is useful to determine the dynamic behavior of the model before executing the optimum design.

The program was developed on a Digital Equipment VAX cluster at NASA Lewis and was executed interactively in case of a smaller model (e.g., a beam or a plate). On the other hand, in case of a larger model such as a gearbox, the program was submitted to a CRAY XMP/28 supercomputer. The program is coded in FORTRAN77, and no particular hardware or software is required; therefore, users can modify it to introduce other methods of optimization, different finite elements, and so forth.

## Accuracy of Numerical Solutions

Validating REVISE has two aspects: verification of the numerical solution method and the estimation of errors. Estimation of the errors requires experimental data, and some comparisons to measured values are presented later with the results of the gearbox optimization. However, verification of the numerical method can be accomplished by comparing numerical solutions of problems to exact analytical solutions. Following are results from a few simple examples solved to verify the accuracy of the finite element and modal analysis solutions calculated by the computer program. The material constants used were modulus of elasticity E = 206 GPa, Poisson's ratio $\nu = 0.3$, mass density $\rho = 8000$ kg/m$^3$, and coefficients for defining the proportional damping matrix $\alpha = 1.0$ s$^{-1}$ and $\beta = 5.0\times10^{-7}$ s.

Static Bending of a Simply Supported Square Plate.—Table I shows the numeric solutions and the exact analytical solutions for the maximum deflections of a simply supported square plate for two loading conditions. One condition is the deflection caused by a central-concentrated load P and the other is the one caused by a uniformly distributed load $pL^2$. The solutions for deflections converge well toward the exact values, and the error of the numeric solution is less than 1 percent even for the case a coarse mesh of 8×8×2 elements.

Static Bending of a Cantilever Plate.—Jaramillo (ref. 15) obtained the exact analytical solutions for the deflection and bending moment of a cantilever plate with infinite width and a concentrated load. His result shows that the deflection diminishes rapidly as the distance from the loading point increases, and the deflection becomes a negligibly small value at a position along the width of more than three times the length. Therefore, a plate with a width six times its length may be considered approximately as a plate of infinite width. Such a plate was divided into an 8×32×2 mesh, and the numerical solutions were obtained. Comparing the numerical solution to the analytical solution of Jaramillo, the maximum deflections were within 1.8 percent of each other. The maximum bending moments were within 4.7 percent of each other.

Static Analysis of a Cylindrical Shell.—Scordelis and Lo (ref. 16) obtained the analytical solution for the deformation of a cylindrical shell caused by its weight. The numerical solutions are compared with their analytical solutions in figure 3. The maximum deflection is close to the analytical solution. On the other hand, the circumferential bending moment is about 10 percent less than the analytical solution. Such errors for the bending moment is typical for finite-element solutions by the displacement method as used here.

Eigenvalue Analysis of a Simply Supported Rectangular Plate.—A rectangular plate, 600- by 400-mm and 5-mm thick, was divided into meshes of 4×4×2, 6×6×2, and 8×8×2 dimensions. A similar mesh pattern was later used to optimize a gearbox housing. The computed natural frequencies of the plate are shown in table II. In the table, the mode shape indication of (m,n) means the mode shape has m-1 and n-1 nodal lines along the two sides. The results of the numerical computations are mostly smaller than the analytical solutions, with the error depending on the mode shape and order. To provide another comparison, the arithmetic mean of the squared error was calculated, and its square root is illustrated in figure 4. Based on this arithmetic mean error, if a 6 percent precision is desired, then a 6×6×2 mesh of elements is sufficient for solutions of modes up to 10th order.

The numerical solutions of the previously described sample problems showed good agreement with analytical solutions, thereby demonstrating and verifying the finite element and modal analysis done via REVISE.

## OPTIMUM DESIGN OF BEAMS AND PLATES

To illustrate the optimization process and verify REVISE, the optimum shapes of beams and plates were computed. The material constants used were modulus of elasticity $E = 206$ GPa, Poisson's ratio $\nu = 0.3$, mass density $\rho = 8000$ kg/m$^3$, and coefficients for defining the proportional damping matrix $\alpha = 1.0$ s$^{-1}$ and $\beta = 5.0\times10^{-7}$ s.

### Optimum Shapes of Beams

Because the element used in this research is not a beam but a shell element, the computer program is not specifically suited for beam analysis. However, a sufficiently narrow-width plate can approximate a beam, and is referred to as a beam in this section. The pattern of the finite-element mesh is shown in figure 5. The beam is first divided into a 10×2 mesh of equal rectangles, and then each rectangle is subdivided into two triangles such that the pattern is symmetrical. The element numbering is shown in figure 5. The beam dimensions are length $L = 200$ mm, width $W = 10$ mm, and initial thickness $t_0 = 5$ mm.

Simply Supported Beam.—Comparing the numerical solution of the eigenvalue problem to analytical solutions, the first four natural frequencies and their errors are 288.9 Hz (0.5 percent), 1172 Hz (1.9 percent), 2704 Hz (4.5 percent), and 4982 Hz (8.3 percent), respectively. With the center of the beam excited by a unit harmonic force, the frequency response of the vibration energy was evaluated numerically at every 10 Hz using the first four modes. This result is illustrated by the broken line in figure 6 with the abscissa representing the excitation frequency. The peak in the figure shows the resonant response of the fundamental natural mode whose frequency is 288.9 Hz. The beam's vibration energy of about $0.207\times10^{-7}$ J in response to a unit harmonic force of 270 Hz applied at the center is considerably high because of the influence of resonance.

The optimum design was calculated to minimize the vibration energy when excited by the 270 Hz frequency force and with the upper and lower limits for the beam thickness constrained to be $1 \le t \le 10$ mm. At each iteration of the optimization procedure, the beam's response energy was calculated and normalized to that of the initial beam of constant thickness. The trend of the normalized response energy with iteration number is shown in figure 7. The energy decreases rapidly and converges to about one tenth of the initial energy after four iterations. The frequency response of the optimally designed beam is indicated by the solid line in figure 6. The fundamental natural frequency was shifted from 288.9 to 319.7 Hz.

The optimum shape of the beam is illustrated in figure 8. The thickness is greatest at the center and gradually decreases towards the supported ends. The shape of the optimized beam is compared to the shape of a beam of uniform strength in figure 9. The latter is well known as the optimum shape for maximum stiffness under static load (ref. 17). Though the thicknesses near the loading points differ, the overall shapes of the beams are very similar. Another optimum shape, obtained by using a more dense finite element mesh of 20×2×2, is also shown in the figure. It is approximately the same shape as obtained for the coarse 10×10×2 mesh.

In the above optimizations, the four elements across the beam width, (e.g., elements 1 to 4 in figure 5) were forced to equal thicknesses. Eliminating that constraint from the optimization procedure, we obtain the optimum shape illustrated in figure 10. At most locations, the beam thickness is at the higher or lower constraint limits. However, the tendency that the thicknesses decrease toward the supporting ends is the same as the former examples. The variation of element thickness as a function of the number of optimizing iterations is summarized in table III. In

the first few iterations, the element thicknesses across the beam width are very close to each other, then, as more iterations are completed, the thicknesses gradually expand.

The frequency response and the convergence of the total vibration energy are shown in figures 11 and 12, respectively. As compared with the former examples of constant thickness across the beam width, more iterations are needed for convergence to the optimum shape. Also, the total vibration energy is reduced by a greater amount. The beneficial effect of the optimized beam shape is illustrated in the continuative vibration amplitude plot responses to a unit harmonic force, figure 13. These responses were evaluated numerically by the method described in the Modal Analysis of Forced Vibration section. The response amplitude was reduced by an additional order of magnitude for the second optimization, allowing thickness variation across the beam, compared to the first optimization with constant thickness across the beam's width.

As another example, the vibration energy at 2680 Hz was minimized for the same simply supported beam. This excitation frequency is a little lower than the third natural frequency. First, the thickness across the beam was constrained to be uniform and the optimized shape was calculated. Figure 14 shows the frequency responses of the total vibration energy before and after the optimization, and the convergence of the energy is shown in figure 15. The optimum shape is illustrated in figure 16. The thicknesses near the nodes of vibration are decreased by the optimization method. Next, the beam thickness across the width was allowed to vary, and the optimized shape recalculated. The thickness distribution of the optimized shape, shown in figure 17, is almost same as the first optimization, figure 16. The frequency response and the convergence of the energy for the second optimization are shown in figures 18 and l9, respectively. The resonance peak shifts to a much higher frequency for the second optimized shape, figure 18, compared to the first, figure 14. The continuative vibrations of the original beam and the two optimized shapes, figure 20, dramatically illustrates the benefit of the optimization procedure to reduce vibrations.

Clamped Beam.—As another sample problem, a beam with the same geometry as discussed in the Simply Supported Beam section, but with clamped rather than simply supported ends was studied and optimized. The first four natural frequencies of the initial beam with constant thickness were calculated numerically as 671.2, 1904, 3887, and 6787 Hz. These numeric solutions are not quite as accurate as those for the simply supported beams. The frequency response of the initial-thickness beam was evaluated using only the first four modes. The frequency response is shown in figure 21. Next, the beam was optimized to minimize the vibration energy at 650 Hz, which is slightly lower than the first fundamental natural frequency.

The thickness across the width of the beam was constrained to be equal for the first optimization. The convergence of the energy is shown in figure 22. More iterations are required for convergence as compared to the optimization of the simply supported beam. The optimum shape of the beam is illustrated in figure 23. The thickness increases slightly at the center and greater at the fixed ends. These positions correspond to positions of maximum bending moments. The optimum shape of the clamped beam was compared with the shape of a beam of uniform strength, figure 24 and the shapes were found to be similar. However, the shape optimized for minimum vibration has a greater thickness near the fixed ends while the uniform strength beam is thicker near the center. The difference seems to be effective in reducing vibration.

A second optimization of the clamped beam was done, eliminating the constraint of equal thickness across the width. The optimum shape is shown in figure 25. The mean thickness for each group of four elements across the beam width are close to the thickness distribution of the first optimized shape. The frequency response of the vibration energy and the convergence of the optimization are shown in figures 26 and 27. Comparing figure 21 to figure 26, the resonance peak is shifted much higher in the case of allowing rather than constraining thickness variation across the beam width, leading to a lower energy level. Figure 28 shows the amplitudes of continuative vibration of the original and two optimized clamped beams. The amplitude is reduced greatly by the optimization. In figure 28, the slope at the clamped end is not zero because the amplitudes at the nodes are connected by straight lines rather than curved. Therefore, the slope not equal to zero is not indicative of poor solutions.

## Optimum Shape of Plates

As another sample problem, the optimum shape of a rectangular plate was calculated. The plate size, figure 29, was 600- by 400-mm with an initial thickness $t_0$ of 5 mm. To define the finite-element mesh, the plate was first divided into a 6×6 set of equal rectangles. Then, each rectangle was subdivided into two triangles such that the pattern was symmetrical (fig. 29). The element thicknesses were constrained to be $2 \leq t \leq 10$ mm for optimization.

Before executing the optimization calculations, we solved the eigenvalue problem and determined that the first twelve modes were needed to fully cover the frequency range of interest.

Simply Supported Rectangular Plate.—The first optimization of the plate was done for simply supported edges and excitation by a central unit harmonic force. The exciting frequency was 370 Hz, which is slightly lower than the natural frequency of mode (3,1), 376 Hz.

Before executing the optimization, the frequency response of the plate with initial constant thickness was evaluated at every 10 Hz up to 1000 Hz considering only the first twelve modes. The result is shown by the broken line in figure 30 with the abscissa indicating the excitation frequency. The peak near 380 Hz is the resonant response of mode (3,1), and therefore, the energy at the excitation frequency of 370 Hz is high, about $0.338 \times 10^{-4}$ J. Next, the optimized shape was calculated. The convergence of the vibration energy as a function of iteration number is shown in figure 31, with the response energy shown as a ratio to that of the first iteration. The energy decreases sharply on the first iteration and converges to about 1/1000th of the initial energy after eight iterations. The frequency response of the optimized design is represented by the solid line in figure 30. The location of mode (3,1) shifts to about 520 Hz, thus greatly reducing the vibration energy at the exciting frequency.

The optimum shape of the plate is illustrated in figure 32. The major change is an increase in thickness of the elements along the longer center line. The area seems to function as a stiffener, which leads to the reduction of modal vibration (3,1). The decrease in thickness at the nodal line that was observed in the optimization of the simply supported beam (fig. 16) is not observed in this simply supported plate example.

A second optimum shape was calculated, in this case for an exciting force at 390 Hz, which is a little higher than the natural frequency of mode (3,1). The calculated optimal shape is illustrated in figure 33. The frequency response and the convergence of energy are shown in figures 34 and 35, respectively. In this example, the thickness increases at the central portion of the plate rather than along a line as in the previous example. The central portion appears to function as a mass, and the natural frequency of mode (3,1) is shifted by the optimization to a lower frequency, about 314 Hz (fig. 34).

Comparing the frequency responses of the two optimized shapes (figs. 30 and 34), the energy at the excitation frequency is higher for the case of $f_{ex} = 390$ Hz. This demonstrates that the minimized energy obtained for this excitation is a local minimum. These results also indicate that in this example, for the purpose of reducing vibrations in a frequency band that includes the mode under consideration, a shift of a natural mode of vibration to a higher-frequency region is preferred, rather than a shift to a lower-frequency region.

Clamped Rectangular Plate.—As a second example of optimization of plates, the same geometry as the previous example was used except the edges were modeled as clamped rather than simply supported. As in the previous example, the plate was excited by a central unit harmonic force. The exciting frequency used was 530 Hz, which is a little lower than the natural frequency of mode (3,1) at 542.6 Hz. The frequency response of the plate with initial thickness of 5 mm is shown by the broken line in figure 36. The energy at 530 Hz was then minimized by the optimization procedure. The convergence of the energy is shown in figure 37. The energy decreases rapidly on the first iteration and is considerably close to the converged value. The frequency response of the optimized plate is shown by the solid line in figure 36 and the peak of mode (3,1) shifts to about 680 Hz.

The optimum shape of the plate is illustrated in figure 38. The thicknesses of elements along the longer center line were increased considerably, acting as a stiffener to control the vibration of mode (3,1). However, the shape is not as conspicuous as compared to the increase in thickness for the optimum shape of the simply supported plate. The thickness of the optimized clamped plate is small at the edges, similar to the effect seen for the clamped beam solution.

The clamped plate was again optimized, this time for an exciting force with a frequency of 550 Hz. The optimum shape obtained is shown in figure 39. Since the exciting frequency is slightly higher than the natural frequency, the optimization shifts the natural frequency to a lower-frequency region in the same way as the simply supported plate. The thickness increases at the central portion of the plate and appears to have the function of a tuning mass. This characteristic is more clear in comparison with the optimum shape in figure 33. Figures 40 and 41 show the frequency response and convergence of energy, respectively, for this second optimization of the clamped plate. The optimization needs more steps to obtain the solution compared to the case of simply supported edges.

In comparing the results for this example shown in figure 40 with those of figure 36, we conclude that the shift of natural frequency to a lower-frequency region is slightly better than the shift to a higher-frequency region if the objective is just limited to minimize the energy near the natural frequency of 542.6 Hz. This is opposite to the result discussed in the simply supported plate section. However, the difference of the energies is small in this case. Therefore, other considerations might be considered in this case for selecting one optimized design over the other.

In this chapter, the developed computer code for optimization was applied to the design of beams and plates. Clear reductions in vibration through optimization was confirmed by these studies. The optimal shapes have areas of increased thickness that act as either a stiffener or a mass. If the frequency of vibration to be minimized is slightly lower than the frequency of a nearby natural mode, then this method shifts the frequency of that mode to a higher-frequency region. Consequently, since the opposite is also true, this fact can be used to control the direction of the natural frequency shift.

The optimized design should be examined as to whether it is the local minimum. In some cases, shifting the natural frequency in the opposite direction can yield further significant reductions in vibration. The results of this method are somewhat similar to the usual method of avoiding resonance by shifting the natural frequency through strategically locating stiffeners or masses. However, the advantage of using this optimization code is that the user need not design or locate the stiffener or mass. The procedure both calculates the shifting of the natural frequency and also automatically designs and locates the stiffener or mass.

## REDUCTION OF GEARBOX VIBRATION

### Modeling and Eigenvalue Analysis of Gearbox

The optimization procedure was applied to the experimental gearbox of the gear noise rig at NASA Lewis (ref. 5). The origin of a global X, Y, Z coordinate system was defined at the center of the bottom plate with the Y axis parallel to the gear shafts and with the Z axis normal to the bottom plate. The wall center distances of the gearbox were approximately X = 324 mm, Y = 248 mm, and Z = 270 mm. The box was modeled using 256 triangular shell elements. Although more elements would be desired for a more precise analysis, the number of elements was fixed at 256 to limit the required computing resources.

The pattern of the finite-element mesh is shown in figure 42. This gearbox design includes stiffeners and four circular holes for bearings. These structural details, however, were neglected in this model. The mesh is symmetrical about the X axis but not symmetrical about the Y and Z axes. This was done so that the bearing center locations would coincide with a nodal point. For boundary conditions, the four bottom corners of the gearbox were fixed in all directions. The material constants used were modulus of elasticity E = 206 GPa, Poisson's ratio $\nu = 0.3$, mass density = 8000 kg/m$^3$, and coefficients for defining the proportional damping matrix $\alpha = 1.0\ s^{-1}$ and $\beta = 5.0 \times 10^{-7}$ s.

The six surfaces were identified by the numbers 1 through 6 as follows: surface 1 is the top, 2 is the plate at Y = 124, 3 is the plate at X = 162, 4 is the plate at Y = −124, 5 is the plate at X = −162, and 6 is the bottom. Surfaces 2 and 4 support the shafts. The thicknesses of the elements near the bearing locations ($-121 < X < 82$ and $66.5 < Z < 193.5$) were 22.4 mm with the other elements being 6.3-mm thick.

Before calculating the optimum design, the eigenvalue problem was solved to determine the dynamic characteristic of the gearbox (see table IV for the result of the eigenvalue study). The mode shape is represented as ($m_x$, $m_y$) indicating that (m+l) and (m+l) nodal lines are observed in X and Y directions. Sketches of the mode shapes are shown in figure 57. Comparing the calculated results to experimental measurements (ref. l), the calculated fundamental natural frequency at 475 Hz is about 4.4 percent less than the measured value. Though other measurement data is available in reference 1, none of the other measured modes coincide with the results of the calculations. This may be a result of neglecting the effects of stiffeners and shafts in the structural model used for this research.

### Vibration of Gearbox Caused by Harmonic Exciting Forces

Unit-exciting forces were used in this research. Since the gear system's exciting frequencies may be estimated by spectral analysis of the force, the problem may be considered as harmonic forced vibration of the gearbox.

The gearbox vibration response to harmonic excitation was computed for unit harmonic forces applied at the bearing positions in the direction of the gearing line of action. The total vibration energy was calculated at every 10 Hz in the region of 500 to 1500 Hz. In addition, the contribution of each gearbox surface to the total gearbox energy was computed over the same frequency range (see fig. 43). Ten peaks of resonance are seen in the figure at

approximately 540, 580, 610, 770, 940, 1240, 1280, 1320, 1400, and 1460 Hz. The figure also shows the magnitude of vibration energy at these resonance frequencies and the contribution of each surface. For example, it is clear that the vibration energy at 940 Hz is mainly caused by the vibrations of the top and bottom plates.

Of course, the mode shape obtained by the eigenvalue analysis gives only the shape and not the magnitude of the vibration response. In other words, it represents the relative displacement at the nodes. However, all the eigenvectors calculated in this analysis were normalized with respect to the mass matrix. Therefore, if the component related to a certain node is picked up from every mode shape, it might represent the contribution of the mode to the relative magnitude of displacement. The components of displacement at the positions of the bearings were collected from the results of the calculations and normalized with respect to the maximum value to obtain relative displacements. The results, normalized as the ratio to the maximum value, are illustrated in figure 44. For example, figure 44 (a) shows both the displacement in the direction of the X axis and the rotation about the Z axis at the position of bearing 1. The abscissa indicates the order of mode from 1 to 30. The figure shows that the maximum displacement in the direction of X axis originates from the 27th mode shape.

The displacements $u_1$, $w_1$, $u_2$, and $w_2$ were defined as u and w being the displacements in the direction of X and Z axes with subscripts 1 and 2 indicating the positions of bearings 1 and 2, respectively. The resonant frequencies were then obtained from figure 44. In case of spur gears, the work done, U, by the unit load, which is applied at the position of bearings along the line of action, can be estimated by the following expression

$$U = \left|u_1 - u_2\right| \sin \alpha + \left|w_1 - w_2\right| \cos \alpha \tag{55}$$

where $\alpha$ is the operating pressure angle. The work done is also the energy input into the gearbox by the exciting force. Therefore, it should have a strong correlation to the vibration energy of the gearbox. Figure 45 shows this comparison for the ten resonant frequencies. The vibration energy is approximately proportional to the calculated work done even though the calculation is not the actual value but the relative work. This figure suggests that the magnitude of gearbox vibration is sufficiently estimated from the relative work, i.e. from the results of the eignvalue analysis.

## Optimum Design of Gearbox

Top Plate of Gearbox.—The gearbox considered here is made of four side plates and a bottom plate welded together along with a top plate that is bolted in place. Therefore, strictly speaking, the gearbox model should consider and include the function of the bolted joints. However, such a model would have a very complex formulation. To simplify the formulation, the bolted connections were neglected, and the gearbox was modeled as a simple box with all surfaces continuously connected.

First, the eigenvalue problem for the gearbox was analyzed, and the first 30 modes were selected for use in the forced-vibration analysis. Next, the forced-vibration response for the gearbox with all plates at their initial thickness was calculated. The response was calculated in the range of 400 to 2400 Hz for unit harmonic exciting forces applied at the bearing locations and in the direction of the gearing line-of-action. The calculated response in terms of vibration energy is shown by the broken line in figure 46(a), and details of the response in a 500- to 1500-Hz range are shown in figure 46(b). Next, the optimal shape of the top plate was calculated to minimize the response to an exciting frequency of 1260 Hz. This frequency coincides with the gear mesh frequency when the test gears of 28 teeth operate at 2700 rpm. The vibration energy of the initial design at this frequency is about $0.976 \times 10^8$ J. This energy decreases to about 1/5 of this initial value after six iterations of optimization as shown in figure 47. This solution was executed on a CRAY XMP/28 computer system, taking approximately 34 sec of cpu to compile with the CFT77 compiler and 875 sec of cpu for completing the optimization. The frequency response after optimization is shown by the solid line in figure 46. The peak of resonance at 1280-Hz moves to about 1320 Hz.

Assessing the entire frequency range, the variation of the response looks small. However, the energy is greatly reduced at 1200 to 1300 Hz. The optimum shape of the top plate is illustrated in figure 48. The thicknesses of the elements increase above bearing 1 and near the edges that connect to surfaces 2 and 4. From figure 44(b), the displacement along the Y axis is large in the 12th mode at 1277 Hz. The increase in thickness tends to control this displacement by increasing the rigidity of rotation around the X axis.

Figure 49 shows the energy share of each surface before and after the optimization. The energy reduction of the top plate is relatively small, however, the changes in the top plate design also produces vibration reductions of the other surfaces. The frequency response of the energy of each surface is shown in figure 50. In these figures, the energy of each surface is compared with the overall energy of the gearbox after optimization. It is clear from the results that the peak of resonance at about 1320 Hz is caused by the vibration of surfaces 2 and 4, and that the new resonance at 1090 Hz is mainly caused by the vibration of the top plate.

Design of Top Plate and Two Side Plates of Gearbox.—Next, the two side plates and the top plate were optimized simultaneously. Side plates 3 and 5 were selected to be varied by optimization, as they do not support the shafts. The condition of excitation used was the same as the previous example, and again, the first 30 modes were considered in the analysis.

The frequency response of the gearbox with initial thickness is shown by the broken line in figure 51. The overall vibration energy of the box was minimized for an exciting frequency of 1260 Hz by allowing the element thicknesses of the top and two side plates to vary. The frequency response after optimization is shown by the solid line in figure 51. The energy is reduced considerably in the region of 1180 to 1370 Hz. The reduction of vibration energy is larger than the first example, where only the design of the top plate was varied.

The optimization converges such that the response energy is about 1/30 of the initial value as shown in figure 52. The optimum shapes of the top plate and two side plates are illustrated in figure 53. The thickness distribution of the top plate is similar to the top plate of the first example; however, the weight of the top plate is reduced about 15 percent by the optimization as compared to the initial weight. The optimum shapes of plates 3 and 5 are fairly close to each other. The thicknesses increase toward the bottom corners of the side plates. The weight of plate 5 is reduced by 7 percent while the weight of plate 3 increases about 23 percent. The total weight of the gearbox was constrained to be equal.

Figure 54 shows the energy share of each surface before and after optimization. The energy reduces for every surface, but the reduction for plate 3 is most remarkable. The frequency response of the energy in each surface is shown in figures 55 and 56. Figure 55 shows the contribution of each surface on the total energy, and figure 56 demonstrates the change of frequency response of each surface by the optimization.

## CONCLUDING SUMMARY

A method was developed to reduce gearbox noise via structural optimization of the housing for low vibration. The method is based on the theories of finite elements, modal analysis, and optimization techniques. A three-node, triangular-shell finite element with 18 degrees of freedom was developed and implemented for structural and modal analysis.

For optimization, the element thickness was the design variable, while the overall vibration energy in response to unit harmonic excitation was the objective function to be minimized. The vibration-response energy sensitivity with respect to the design variable was derived and expressed by the sensitivities of eigenvalues and eigenvectors. The optimal designs were constrained to have a constant total weight for the structure. Optimal solutions were computed by the gradient projection method with a unidimensional search procedure. The computer program, REVISE, was written to perform the calculations.

The finite-element and modal analysis parts of REVISE were verified by comparing the numerical solutions to exact analytical solutions for (1) the static analysis of a square plate, cantilever beam, and cylindrical shell, and (2) the eigenvalue analysis of a rectangular plate. Good agreement between the numerical and analytical solutions were obtained.

The optimization procedure was demonstrated by calculating the optimum shapes for minimum vibration response for simply supported and clamped beams and plates. The optimal shapes had areas of increased thickness that acted as either a stiffener or mass. Forced-response analysis of the optimized shapes clearly demonstrated that significant vibration reductions were achieved via the optimization procedure. It was demonstrated that if the vibration frequency to be minimized was slightly lower than a nearby mode, the optimizer will shift the frequency of that mode to a higher region. The opposite is also true. It was also shown that optimized designs should be examined to determine whether the minimum obtained is a local one since, in some cases, further significant reductions in vibration energy can be obtained by shifting the frequency in the opposite direction. The optimizer produces similar

effects to those of the usual procedure of shifting resonant frequencies by strategically adding a stiffener or mass to the design. However, an advantage of using the optimizer is that the stiffener or mass is designed and located automatically.

The computer code was applied to optimize the housing of the NASA Lewis Research Center's gear noise rig test gearbox. Two solutions were obtained: once changing the shape of the top plate only and a second time changing the shape of the top and two side plates simultaneously. The shapes were optimized to minimize the vibration energy in response to unit harmonic forces applied at the bearing locations along the gearing line of action.

The total weight of the structure was constrained to be constant. The solutions of the forced-vibration problem of the gearbox showed that the vibration energy was approximately proportional to the relative work, which was calculated from the bearing forces and the relative displacements estimated from the mode shapes. This suggests that the magnitude of forced vibration is approximately estimated from the results of eigenvalue analysis. Compared to the initial design, optimizing the top plate only reduced the housing vibration energy by about 1/5. The contribution of vibration of each surface to the total vibration was calculated. By viewing the results this way, it was clear that optimizing the top plate not only reduced the vibration of that surface but also of the other surfaces as well. Futhermore, simultaneously optimizing the shape of the top and two side plates reduced the housing vibration energy by about 1/30 compared to the initial design.

## ACKNOWLEDGMENTS

This research was conducted while the first author was a visiting researcher at the NASA Lewis Research Center as a Research Associate of the National Research Council (NRC). The author expresses thanks to the NRC for the opportunity to participate in the NRC program. The research advisor, Dr. John J. Coy, Chief of Mechanical Systems Technology Branch, and Mr. Dennis P. Townsend, Senior Research Engineer, offered the perfect circumstances and facilities for this research. The author feels grateful to them and other members in the Branch.

## REFERENCES

1. Lim, T.C.; Singh, R.; and Zakrajsek, J.J.: Modal Analysis of Gear Housings and Mounts. Proceedings of the 7th International Modal Analysis Conference, Society for Experimental Mechanics, Inc.,vol. II, 1989, pp. 1072-1078.
2. Choy, F.K., et al.: Modal Analysis of Multistage Gear Systems Coupled with Gearbox Vibrations. NASA TM–103797, AVSCOM TR 90–C–033, 1991.
3. Kubo, A.; Kiyono, S.; and Fujino, M.: On Analysis and Prediction of Machine Vibration Caused by Gear Meshing. First Report: Nature of Gear Vibration and the Total Vibrational Excitation. JSME Bull., vol. 29, no. 258, 1986, pp. 4424–4429.
4. Takatsu, N., et al.: Analysis of Experiment on the Vibration Transmission in a Single Stage Gearbox. Proceedings of the International Conference on Motion and Power Transmissions, JSME, 1991, pp. 104–109.
5. Oswald, F.B., et al.: Comparison of Analysis and Experiment for Dynamics of Low-Contact-Ratio Spur Gears. NASA TM–103232, AVSCOM TR–90–C–017, 1991.
6. Seybert, A.F.; and Wu, T.W.: User's Manual, Computer Program BEMAP. Ver. 2.4, Spectronics, Inc., 1989.
7. Atrek, E., et al. Ed.: New Directions in Optimum Structual Design. John Wiley & Sons, 1984.
8. Mota Soares, C.A., Ed.: Computer Aided Optimal Design: Structural and Mechanical Systems. Springer-Verlag, 1987.
9. Hernandez, S.; and Brebbia, C.A., Ed.: Optimization of Structural Systems and Applications. Computational Mechanics Publications, Elsevier Applied Science, 1993.
10. Inoue, K.; Kato, M.; and Ohnuku, K.: Optimum Design of a Plate on the Minimization of the Vibration Energy. JSME Trans., Part C, vol. 56, no. 529, Sept. 1990, pp. 2361–2366.
11. Rosen, J.B.: The Gradient Projection Method for Nonlinear Programming. Part II: Nonlinear Constraints. SMJMA, vol. 9, no. 4, 1961, pp. 514–532.

12. Fox, R.L.; and Kapoor, M.P.: Rates of Change of Eigenvalues and Eigenvectors. AIAA J., vol. 6, no. 12, 1968, pp. 2426–2429.
13. Zienkiewicz, O.C.; and Cheung, Y.K.: The Finite Element Method in Structural and Continuum Mechanics, McGraw-Hill, New York, 1967.
14. International Mathematical and Statistical Library. Math/Library: User's Manual, Mathematical Applications. IMSL Inc., 1991.
15. Jaramillo, T.J.: Deflections and Moments Due to a Concentrated Load on a Cantilever Plate of Infinite Length. J. Appl. Mech., vol. 17, 1950, pp. 67–72.
16. Scordelis, A.C.; and Lo, K.S.: Computer Analysis of Cylindrical Shells. J. Am. Concrete Inst., vol. 6, no. 5, May 1964, pp. 539–561.
17. Huang, N.C.: Optimal Design of Elastic Structures for Maximum Stiffness. Inter. J. Solids Struct., vol. 4, 1968, pp. 689–700.

TABLE I.—DEFLECTION OF SIMPLY SUPPORTED SQUARE PLATE

| Mesh dimension | Loading condition[a] | |
|---|---|---|
| | Concentrated, $w_{max}/(PL^2/D)$ | Distributed, $w_{max}/(PL^4/D)$ |
| Finite element mesh | | |
| 8×8×2 | 0.011636 | 0.004087 |
| 12×12×2 | .011635 | .004081 |
| 16×16×2 | .011633 | .004076 |
| Closed-form solution | | |
| ------- | 0.01160 | 0.004062 |

[a]Flexural rigidity of plate denoted by D.

TABLE II.—NATURAL FREQUENCIES OF SIMPLY SUPPORTED RECTANGULAR PLATE

| Number of nodal lines, n | Mesh dimension | Frequency, Hz | | | | | |
|---|---|---|---|---|---|---|---|
| | | Number of nodal lines, m | | | | | |
| | | 1 | 2 | 3 | 4 | 5 | 6 |
| 1 | 4×4×2 | 103.0 | 198.0 | 380.3 | 659.8 | ------ | ------ |
| | 6×6×2 | 104.9 | 204.1 | 376.1 | 643.2 | 1007 | ------ |
| | 8×8×2 | 105.7 | 205.0 | 376.1 | 624.2 | 969.1 | 1414 |
| | analy.[a] | 108.9 | 209.4 | 376.9 | 611.4 | 912.9 | 1281.4 |
| 2 | 4×4×2 | 310.3 | 383.2 | 539.2 | ------ | ------ | ------ |
| | 6×6×2 | 317.3 | 404.0 | 558.2 | 804.9 | 1130 | ------ |
| | 8×8×2 | 321.2 | 412.4 | 573.4 | 806.6 | 1141 | 1567 |
| | analy.[a] | 335.0 | 435.5 | 603.0 | 837.5 | 1139.1 | 1507.6 |
| 3 | 6×6×2 | 669.6 | 742.6 | 864.0 | 1099 | 1391 | ------ |
| | 8×8×2 | 677.4 | 756.9 | 900.8 | 1115 | 1426 | 1824 |
| | analy.[a] | 711.9 | 812.4 | 979.9 | 1214.4 | 1515.9 | 1884.5 |
| 4 | 6×6×2 | 1169 | 1228 | 1359 | 1555 | ------ | ------ |
| | 8×8×2 | 1173 | 1243 | 1370 | 1538 | 1852 | 2216 |
| | analy.[a] | 1239.6 | 1340.1 | 1507.6 | 1742.1 | 2043.6 | 2412.1 |
| 5 | 8×8×2 | 1810 | 1874 | 1992 | 2180 | ------ | ------ |
| | analy.[a] | 1918.0 | 2018.5 | 2186.0 | 2420.5 | 2722.0 | 3090.5 |

[a]Closed-form analytical solution.

TABLE III.—VARIATION OF ELEMENT THICKNESS OF SIMPLY SUPPORTED BEAM

| Element | Element thickness, mm | | | | | | | | | | |
|---|---|---|---|---|---|---|---|---|---|---|---|
| | Iteration | | | | | | | | | | |
| | 0 | 1 | 2 | 3 | 4 | 6 | 8 | 10 | 12 | 14 | 15 |
| 1 | 5.00 | 3.63 | 2.95 | 2.68 | 1.96 | 1.42 | 1.00 | 1.00 | 1.00 | 1.00 | 1.00 |
| 2 | 5.00 | 3.66 | 2.98 | 2.72 | 2.65 | 4.24 | 4.36 | 4.46 | 4.49 | 5.72 | 5.56 |
| 5 | 5.00 | 4.18 | 4.53 | 4.59 | 5.26 | 6.83 | 7.16 | 7.39 | 7.58 | 9.28 | 9.44 |
| 6 | 5.00 | 4.11 | 4.41 | 4.44 | 3.47 | 1.95 | 1.46 | 1.00 | 1.00 | 1.00 | 1.00 |
| 9 | 5.00 | 4.93 | 5.36 | 5.37 | 3.74 | 1.04 | 1.00 | 1.00 | 1.00 | 1.00 | 1.00 |
| 10 | 5.00 | 5.01 | 5.49 | 5.56 | 6.89 | 8.52 | 8.84 | 9.07 | 9.28 | 10.00 | 10.00 |
| 13 | 5.00 | 5.86 | 5.97 | 6.09 | 7.65 | 9.26 | 9.70 | 10.00 | 10.00 | 10.00 | 10.00 |
| 14 | 5.00 | 5.79 | 5.86 | 5.93 | 4.95 | 2.58 | 1.93 | 1.35 | 1.00 | 1.00 | 1.00 |
| 17 | 5.00 | 6.40 | 6.21 | 6.29 | 6.22 | 5.69 | 5.53 | 5.31 | 4.65 | 1.00 | 1.00 |
| 18 | 5.00 | 6.43 | 6.24 | 6.34 | 7.20 | 8.48 | 9.00 | 9.42 | 10.00 | 10.00 | 10.00 |

TABLE IV.—NATIONAL FREQUENCIES AND MODE SHAPES OF NASA TEST GEARBOX

| Order of eigenvalue | Frequency ($f_i$), Hz | Surface number, nodal lines | | | | | |
|---|---|---|---|---|---|---|---|
| | | 1($m_x$, $m_y$) | 2($m_x$, $m_z$) | 3($m_y$, $m_z$) | 4($m_x$, $m_z$) | 5($m_y$, $m_z$) | 6($m_x$, $m_y$) |
| 1 | 475 | $^{+}$(1,1) | $^{-}$(1,1) | $^{+}$(1,1) | (1,1) | $^{+}$(1,1) | $^{+}$(1,1) |
| 2 | 540 | (1,2) | $^{-}$(1,1) | (2,1) | $^{+}$(1,1) | (2,1) | (1,2) |
| 3 | 543 | $^{-}$(1,1) | (1,2) | (1,2) | (1,2) | (1,2) | $^{+}$(1,1) |
| 4 | 582 | $^{+}$(1,1) | $^{+}$(1,1) | $^{-}$(1,1) | $^{+}$(1,1) | $^{-}$(1,1) | $^{+}$(1,1) |
| 5 | 607 | (2,1) | (2,1) | $^{+}$(1,1) | (2,1) | $^{-}$(1,1) | (2,1) |
| 6 | 768 | $^{+}$(1,1) | $^{+}$(1,1) | $^{+}$(1,1) | $^{+}$(1,1) | $^{+}$(1,1) | $^{+}$(1,1) |
| 7 | 942 | (2,1) | $^{o}$(1,2) | (1,2) | $^{o}$(1,2) | (1,2) | (2,1) |
| 8 | 994 | (2,1) | (2,1) | $^{+}$(1,1) | (2,1) | $^{-}$(1,1) | (2,1) |
| 9 | 1041 | (1,2) | $^{o}$(1,2) | (2,1) | $^{o}$(1,2) | (2,1) | (1,2) |
| 10 | 1101 | (1,2) | $^{o}$(1,2) | (2,1) | $^{o}$(1,2) | (2,1) | (1,2) |
| 11 | 1239 | (3,1) | (1,2) | (1,2) | (1,2) | (1,2) | (3,1) |
| 12 | 1277 | (2,1) | (2,1) | (1,2) | (2,1) | $^{d}$(1,1) | $^{d}$(2,1) |
| 13 | 1321 | (2,1) | (2,1) | (1,2) | (2,1) | (1,2) | (2,1) |
| 14 | 1326 | (1,2) | $^{d}$(1,2) | (2,1) | $^{d}$(1,2) | (2,1) | (1,2) |
| 15 | 1401 | $^{c}$(2 ) | (1,2) | (1,2) | (1,2) | (1,2) | $^{c}$(2 ) |
| 16 | 1406 | (1,2) | (3,1) | (2,1) | (3,1) | (2,1) | (1,2) |
| 17 | 1464 | (2,1) | $^{o}$(3,1) | (1,2) | $^{o}$(3,1) | (1,2) | (2,1) |
| 18 | 1520 | (2,2) | (2,1) | (2,1) | (2,1) | (2,1) | (2,2) |
| 19 | 1538 | (1,2) | $^{d}$(2,1) | (2,1) | $^{d}$(2,1) | (2,1) | (1,2) |
| 20 | 1646 | (2,2) | (1,2) | (2,2) | (1,2) | (2,2) | (2,2) |
| 21 | 1699 | (3,1) | $^{d}$(3,1) | (1,3) | $^{d}$(3,1) | (1,3) | (3,1) |
| 22 | 1788 | (2,2) | $^{d}$(1,2) | (2,2) | $^{d}$(1,2) | (2,2) | (2,2) |
| 23 | 1806 | (3,1) | $^{o}$(3,1) | (1,2) | $^{o}$(3,1) | (1,2) | (3,1) |
| 24 | 1866 | (2,2) | $^{o}$(2,1) | (2,1) | $^{o}$(2,1) | (2,1) | (2,2) |
| 25 | 1923 | (2,2) | $^{o}$(1,3) | (2,2) | $^{o}$(1,3) | (2,2) | (2,2) |
| 26 | 1953 | (3,2) | $^{o}$(1,3) | (2,2) | $^{o}$(1,3) | (2,2) | (2,2) |
| 27 | 2084 | (4,2) | $^{d}$(2,1) | (2,2) | $^{d}$(2,1) | (2,2) | (2,2) |
| 28 | 2112 | $^{d}$( ) | $^{o}$(1,2) | (1,2) | $^{o}$(1,2) | (1,2) | $^{d}$( ) |
| 29 | 2347 | $^{d}$(4,1) | (3,1) | (1,3) | (3,1) | (1,3) | $^{d}$(4,1) |
| 30 | 2448 | (3,2) | $^{o}$(1,3) | (2,2) | $^{o}$(1,3) | (2,2) | (3,2) |

$^{c}$Circular mode shape.
$^{d}$Deformed mode shape.
$^{o}$Oblique nodal line.
$^{+}$Convex outward.
$^{-}$Concave outward.

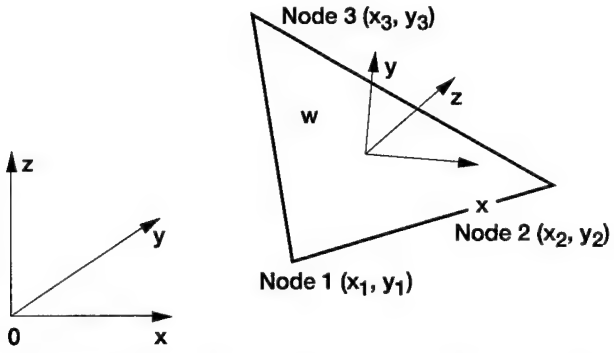


Figure 1.—Shell element in global coordinate system.

| | | | Function |
|---|---|---|---|
| -- Data input | ---------- | RDATA | |
| -- Analyzer | --- ELMMAT | --- LOCAL | (transform to local coordinate) |
| | | --- MASMAT | (form element mass matrix) |
| | | --- STFMAT | (form element stiffness matrix) |
| | --- STATIC | --- STFBND | (form global stiffness matrix) |
| | | --- TRANS | (transform to global coordinate) |
| | | --- LOADNG | (form the load vector) |
| | | --- BCBAND | (introduce boundary conditions) |
| | | --- CHOLSK | (calculate displacements) |
| | | --- STRESS | (calculate stresses) |
| | --- OBJFUN | --- STSSQR | (form global mass and stiffness) |
| | | --- EIGEN | --- CHOL (calculate eigenvalues and eigen- |
| | | | --- HOBS vectors up to given order) |
| | | --- DAMPNG | (calculate modal damping ratio) |
| | | --- ENERGY | (calculate vibration energy) |
| -- Optimizer | --- SENSTV | --- STFMAS | (prepare mass and stiffness) |
| | | --- SENEIG | (calculate sensitivity of eigenvector) |
| | | --- SENDMP | (calculate sensitivity of damping) |
| | | --- SENENG | (calculate sensitivity of energy) |
| | ---------- | GPMACC | (introduce active constraints) |
| | | --- GPMDIR | (calculate feasible direction) |
| | | --- SEARCH | (search the optimum values) |
| -- Output | ---------- | WRHEAD | |
| | | --- WRSTRC | |
| | | --- WRSTAT | |
| | | --- WREIGN | |
| | | --- WROBJF | |
| | | --- WRRESP | |
| | | --- WRSENS | |

Figure 2.—Structure of computer program REVISE. Capital names represent subroutine programs.

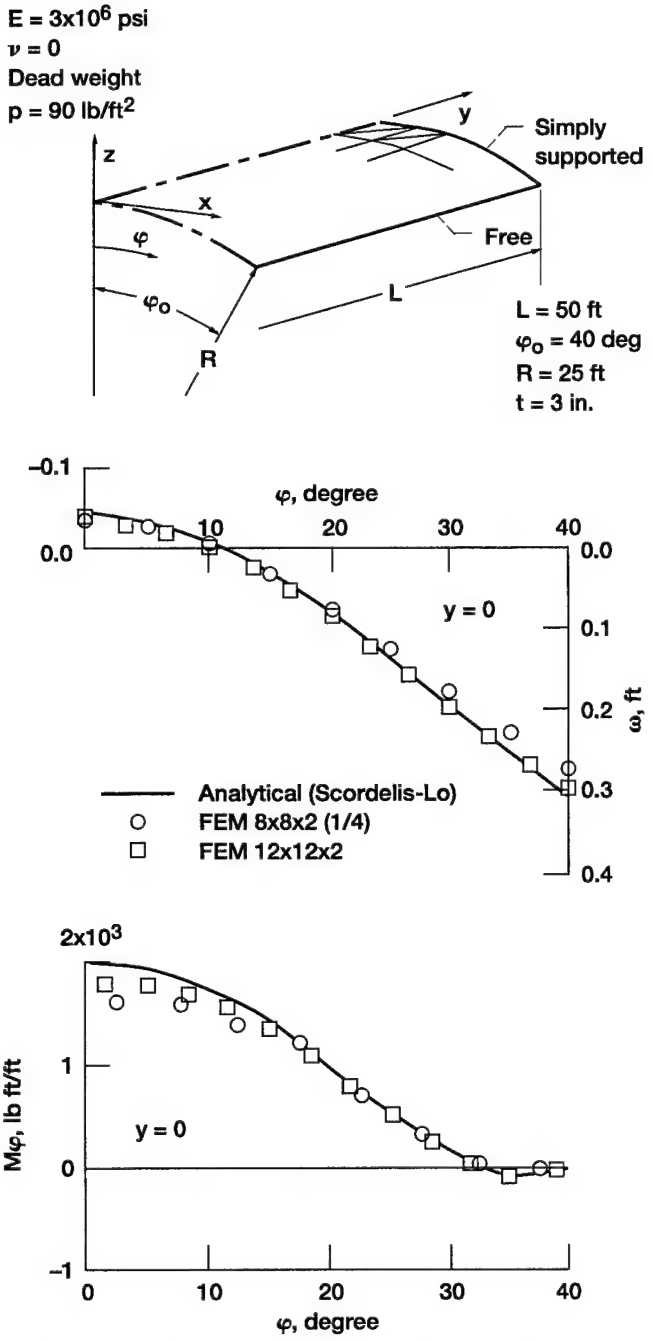


Figure 3.—Deflection and circumferential bending moment of cylindrical shell by finite element and analytical solutions.

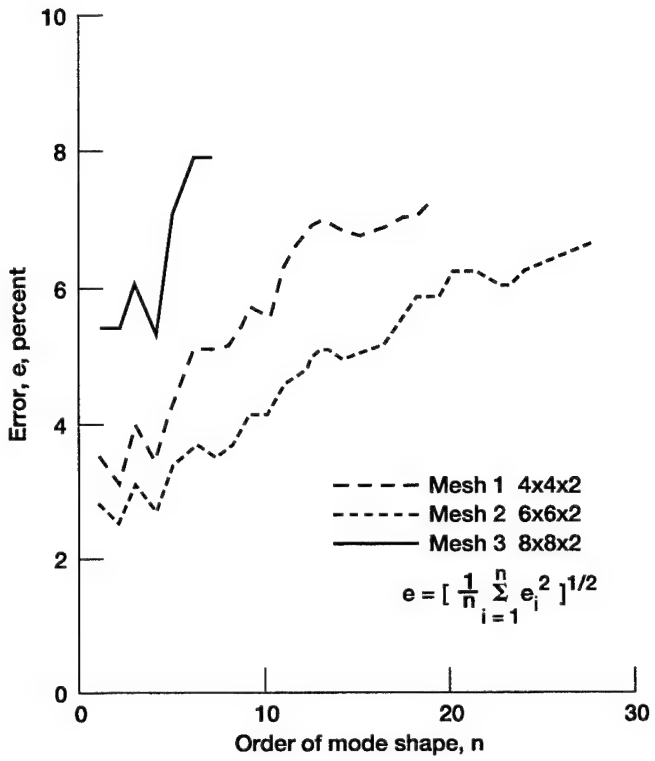


Figure 4.—Error of eigenvalue analysis of simply supported rectangular plate for varying mesh density.

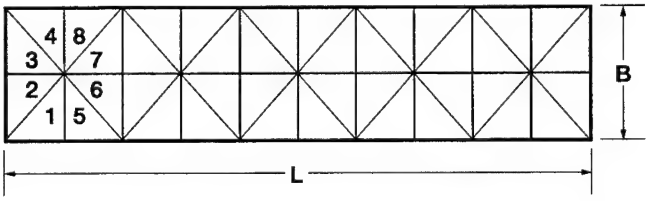


Figure 5.—Pattern of mesh used for optimum design of beam. Length L = 200 mm, width B = 10 mm, initial thickness $t_0$ = 5 mm.

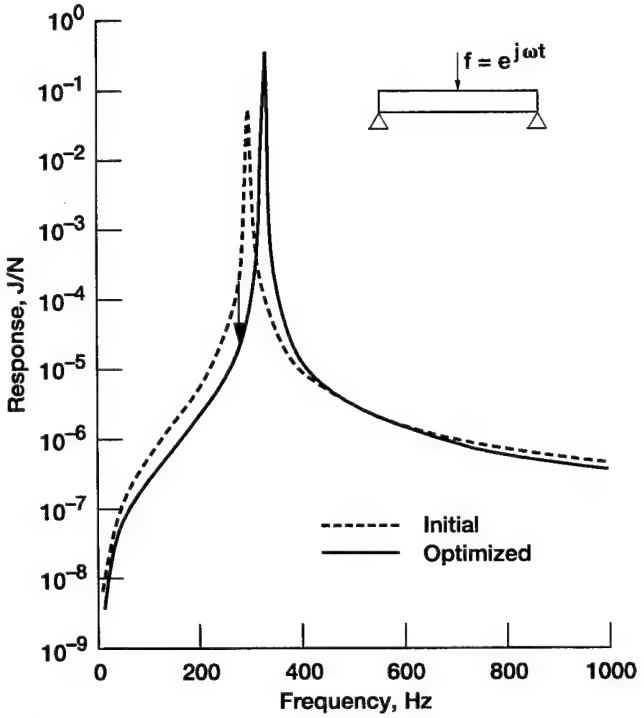


Figure 6.—Frequency response of simply supported beam with constant thickness across width. Excitation frequency $f_{ex}$ = 270 Hz.

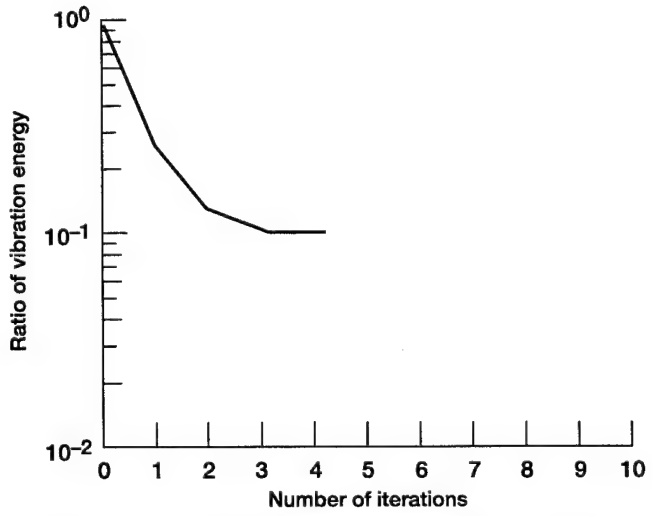


Figure 7.—Convergence of vibration energy by iteration number for optimization of simply supported beam with constant thickness across width. Excitation frequency $f_{ex}$ = 270 Hz.

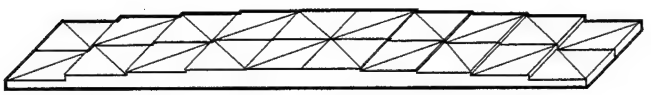

Figure 8.—Optimum shape of simply supported beam with constant thickness across width. Excitation frequency $f_{ex}$ = 270 Hz.

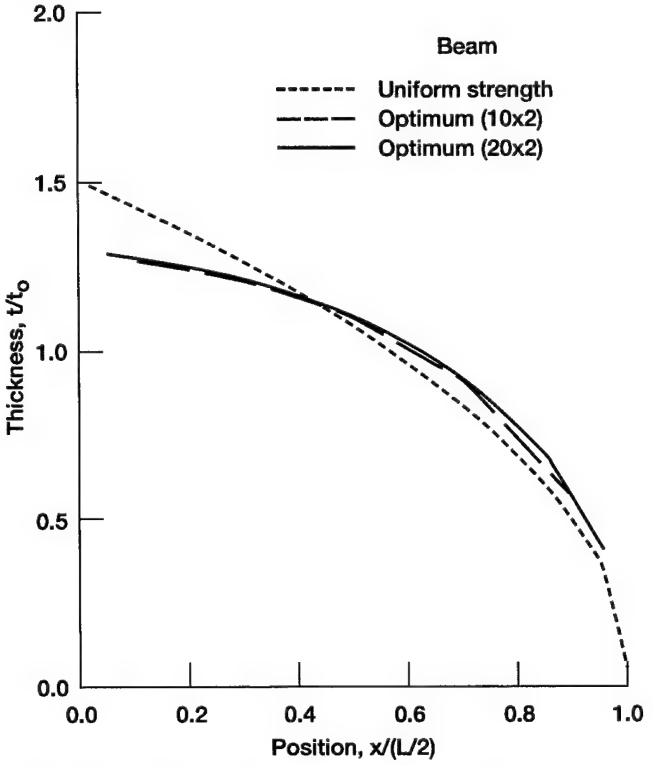


Figure 9.—Comparison of calculated optimum shape for minimum vibration energy and shape of uniform strength beam.

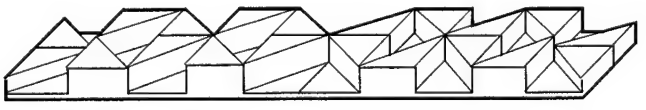

Figure 10.—Optimum shape of simply supported beam with varying thickness across width. Excitation frequency $f_{ex}$ = 270 Hz.

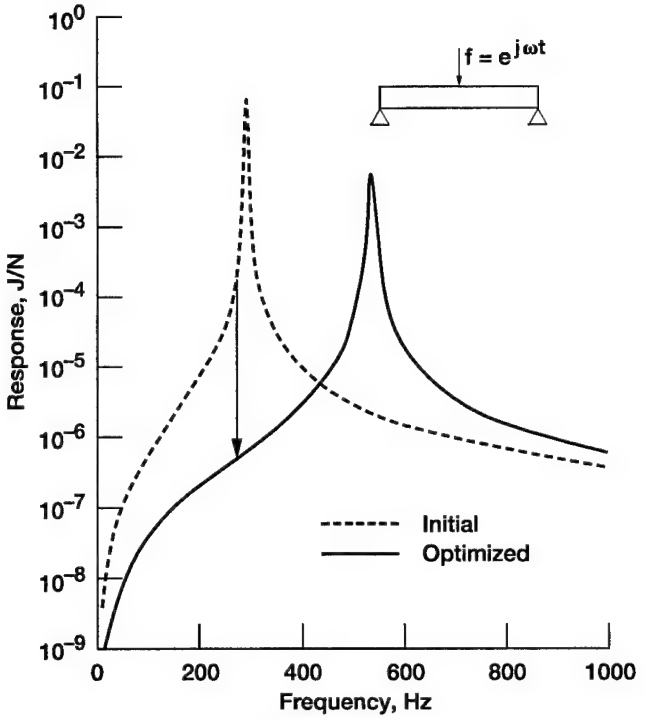


Figure 11.—Frequency response of simply supported beam with varying thickness across width. Excitation frequency $f_{ex}$ = 270 Hz.

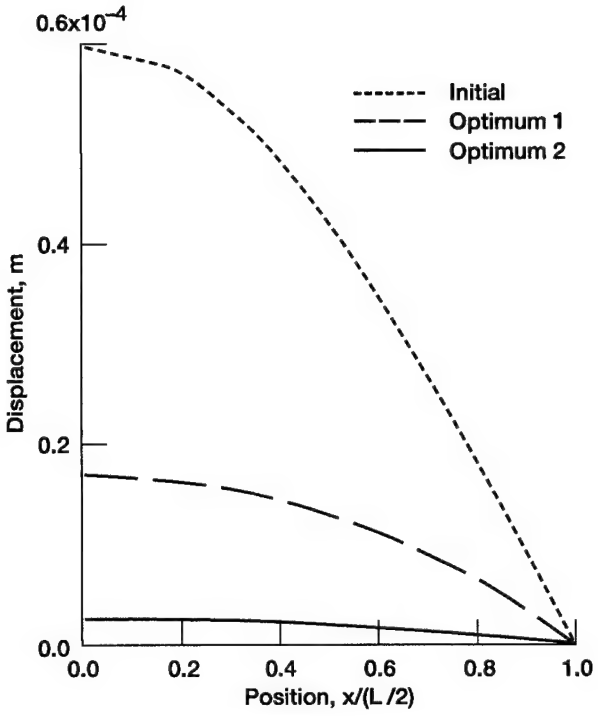


Figure 13.—Displacements due to harmonic excitation (initial; uniform thickness, optimum 1, beam in figure 8, optimum 2, beam in figure 10).

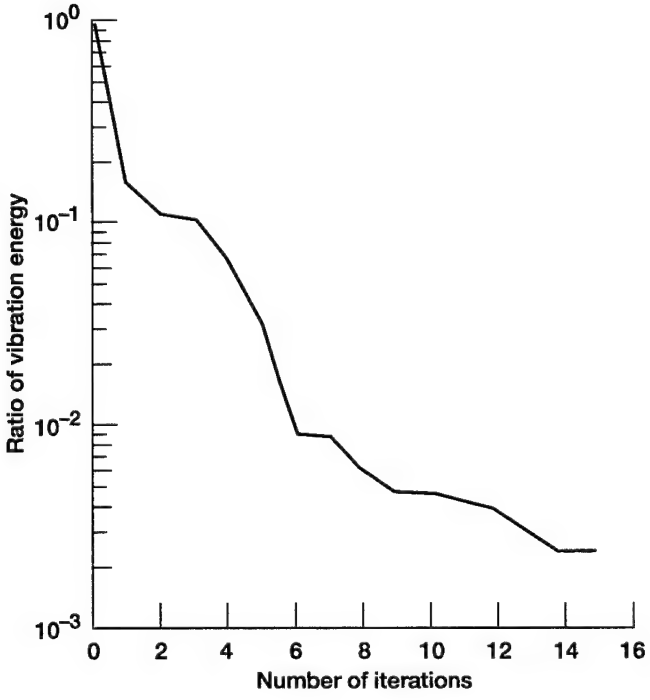


Figure 12.—Convergence of vibration energy by iteration number for optimization of simply supported beam with varying thickness across width. Excitation frequency $f_{ex}$ = 270 Hz.

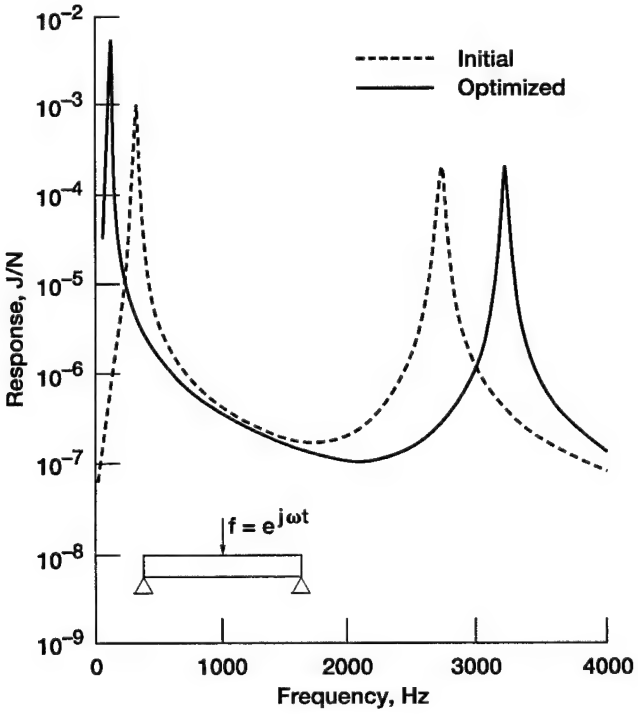


Figure 14.—Frequency response of simply supported beam with constant thickness across width. Excitation frequency $f_{ex}$ = 2680 Hz.

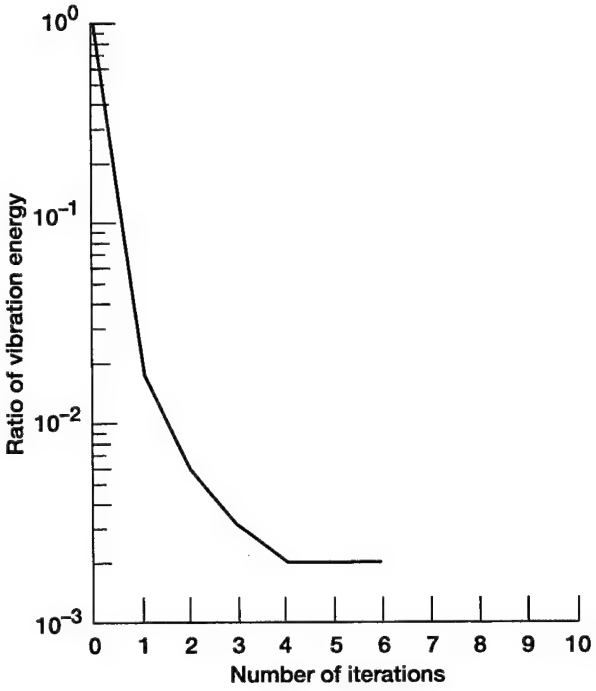


Figure 15.—Convergence of vibration energy by iteration number for optimization of simply supported beam with constant thickness across width. Excitation frequency $f_{ex}$ = 2680 Hz.

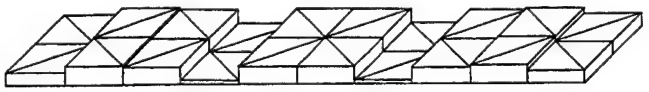

Figure 16.—Optimum shape of simply supported beam with constant thickness across width. Excitation frequency $f_{ex}$ = 2680 Hz.

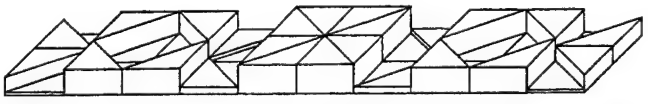

Figure 17.—Optimum shape of simply supported beam with varying thickness across width. Excitation frequency $f_{ex}$ = 2680 Hz.

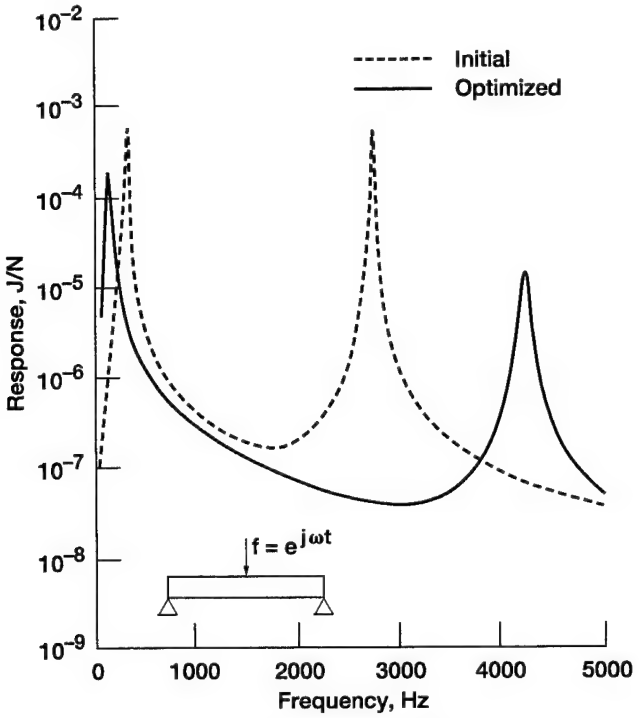


Figure 18.—Frequency response of simply supported beam with varying thickness across width. Excitation frequency $f_{ex}$ = 2680 Hz.

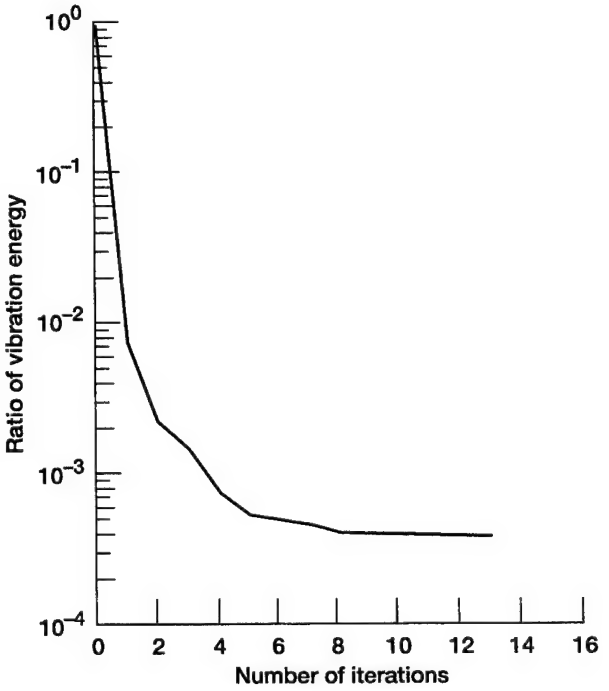


Figure 19.—Convergence of vibration energy by iteration number for optimization of simply supported beam with varying thickness across width. Excitation frequency $f_{ex}$ = 2680 Hz.

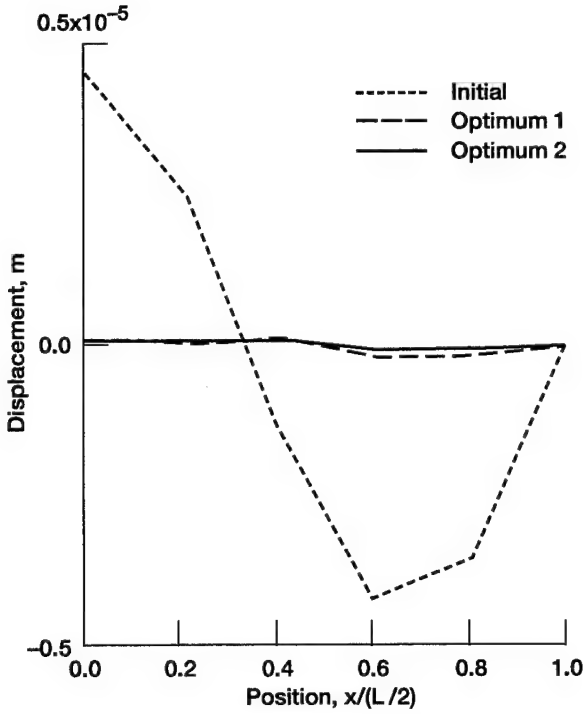


Figure 20.—Displacements due to harmonic excitation (initial; uniform thickness, optimum 1, beam in figure 16, optimum 2, beam in figure 17).

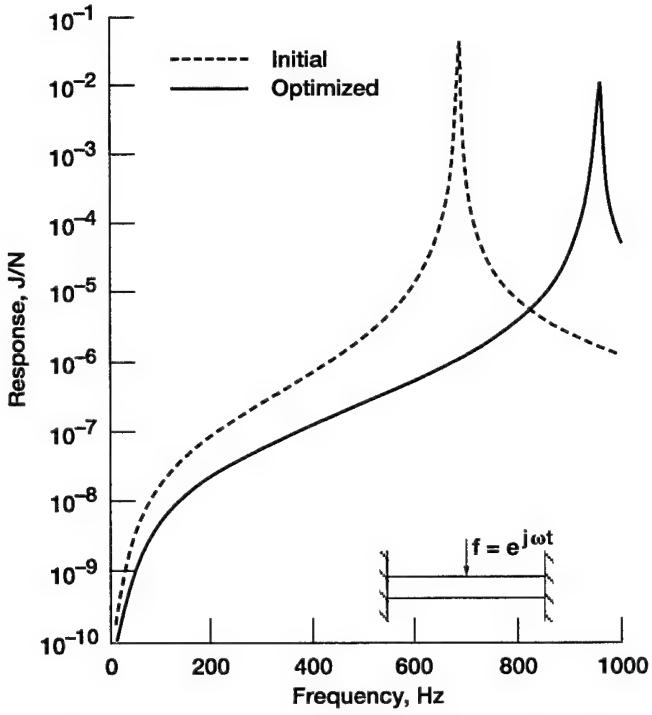


Figure 21.—Frequency response of clamped beam with constant thickness across width. Excitation frequency $f_{ex}$ = 650 Hz.

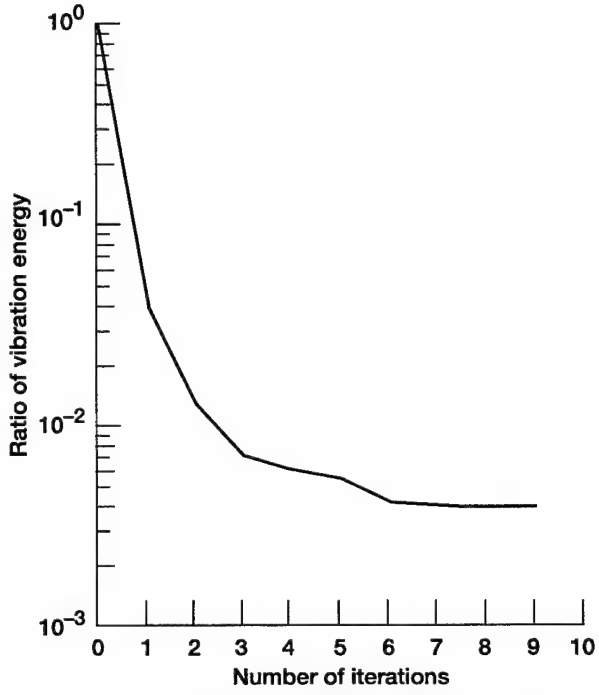


Figure 22.—Convergence of vibration energy by iteration number for optimization of clamped beam with constant thickness across width. Excitation frequency $f_{ex}$ = 650 Hz.

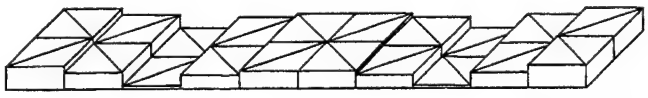

Figure 23.—Optimum shape of clamped beam with constant thickness across width. Excitation frequency, $f_{ex}$ = 650 Hz.

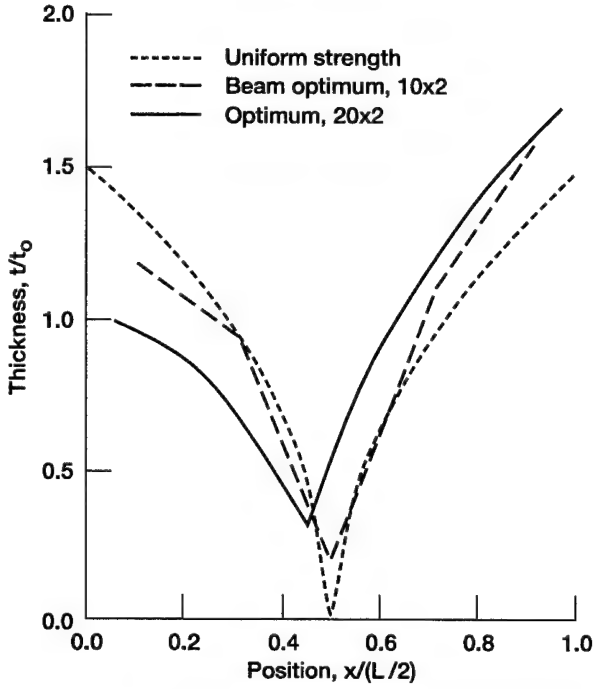


Figure 24.—Comparison of calculated optimum shape for minimum vibration energy with shape of uniform strength beam.

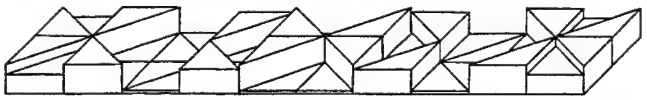

Figure 25.—Optimum shape of clamped beam with varying thickness across the width. Excitation frequency $f_{ex}$ = 650 Hz.

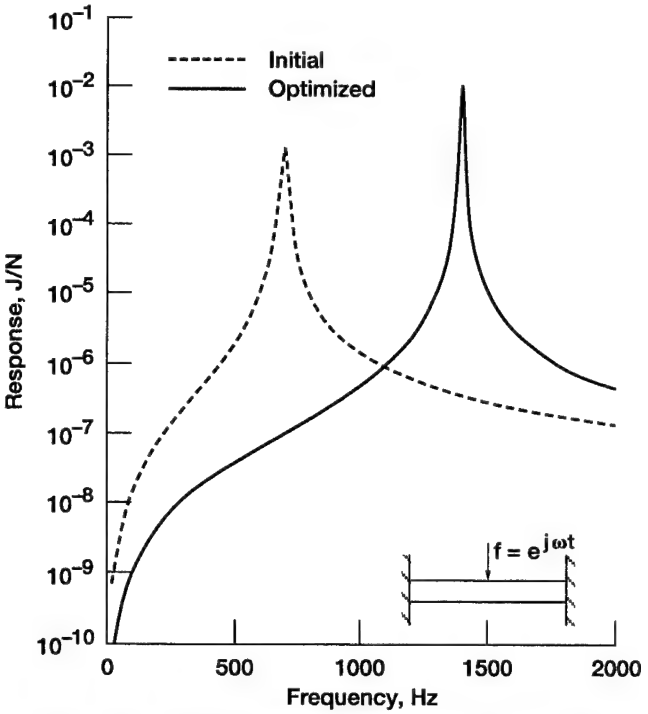


Figure 26.—Frequency response of clamped beam with varying thickness across width. Excitation frequency $f_{ex}$ = 650 Hz.

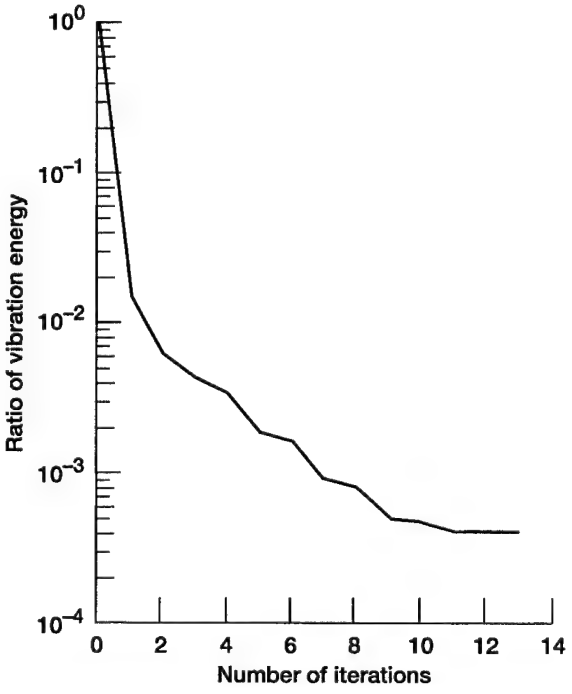


Figure 27.—Convergence of vibration energy by iteration number for optimization of clamped beam with varying thickness across width. Excitation frequency $f_{ex}$ = 650 Hz.

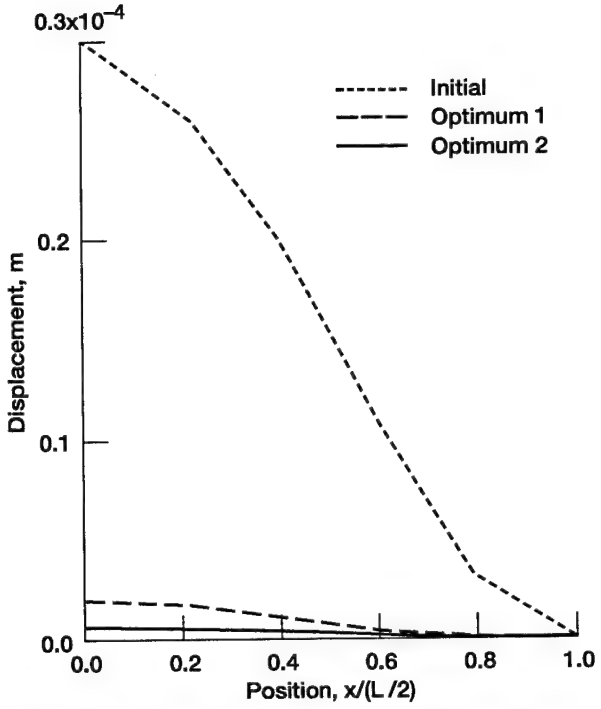


Figure 28.—Displacements due to harmonic excitation (initial; uniform thickness, optimum 1, beam in figure 23, optimum 2, beam in figure 25).

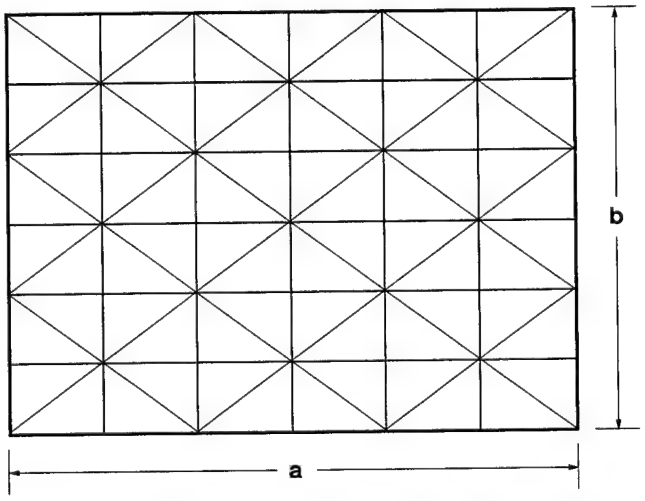


Figure 29.—Pattern of finite element mesh used for optimum plate design (a = 600 mm, b = 400 mm, initial thickness $t_o$ = 5 mm).

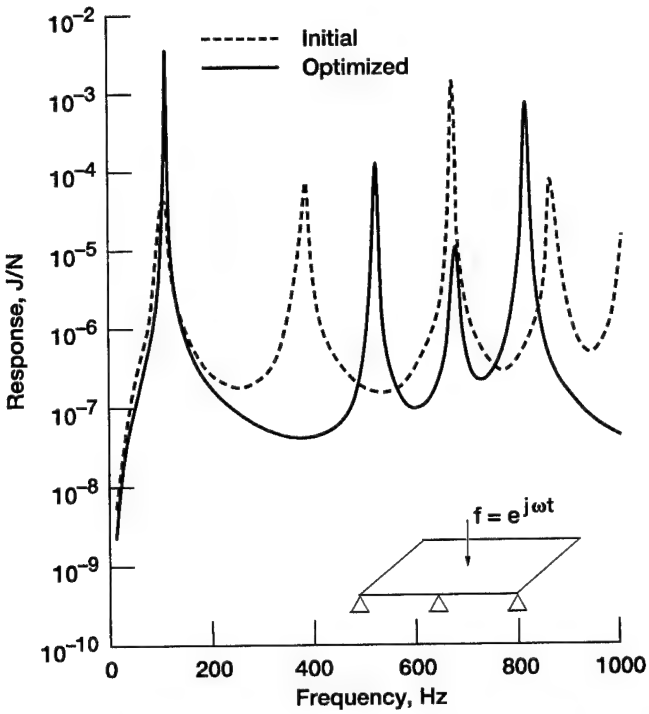


Figure 30.—Frequency response of simply supported plate. Excitation frequency $f_{ex}$ = 370 Hz.

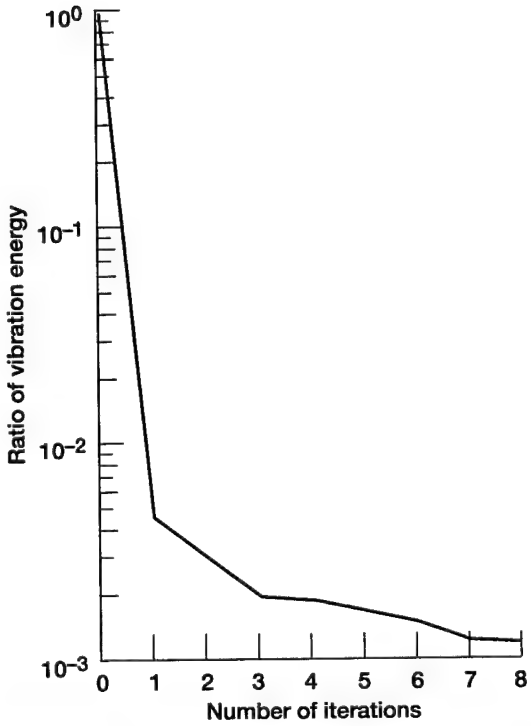


Figure 31.—Convergence of vibration energy by iteration number for optimization of simply supported plate. Excitation frequency $f_{ex}$ = 370 Hz.

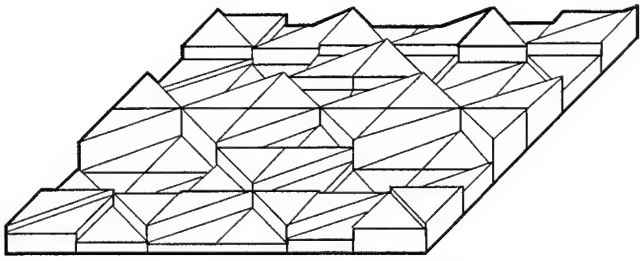

Figure 32.—Optimum shape of simply supported plate. Excitation frequency $f_{ex}$ = 370 Hz.

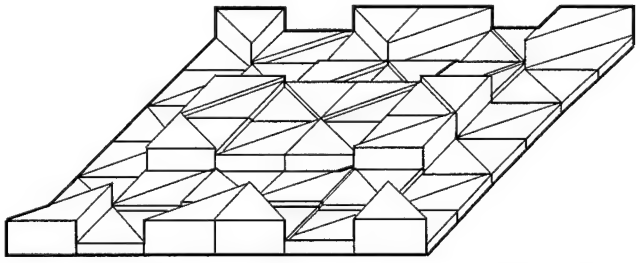

Figure 33.—Optimum shape of simply supported plate. Excitation frequency $f_{ex}$ = 390 Hz.

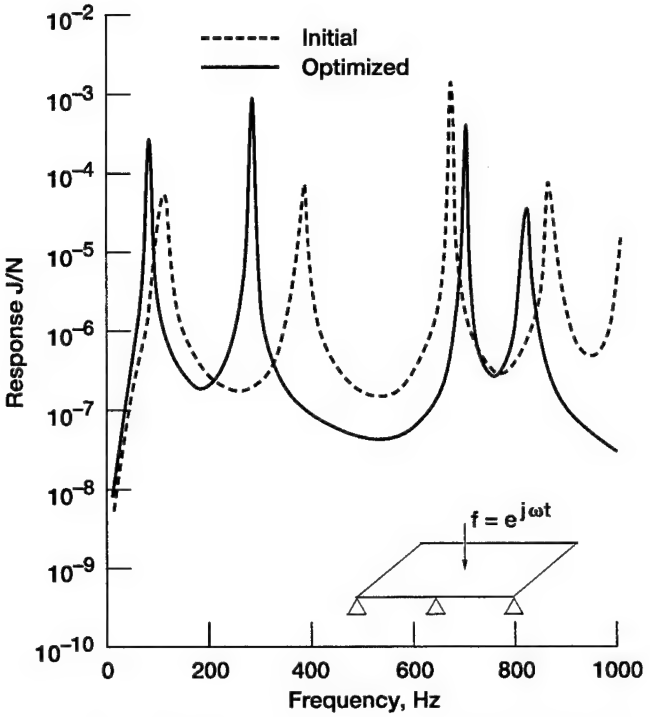


Figure 34.—Frequency response of simply supported plate. Excitation frequency $f_{ex}$ = 390 Hz.

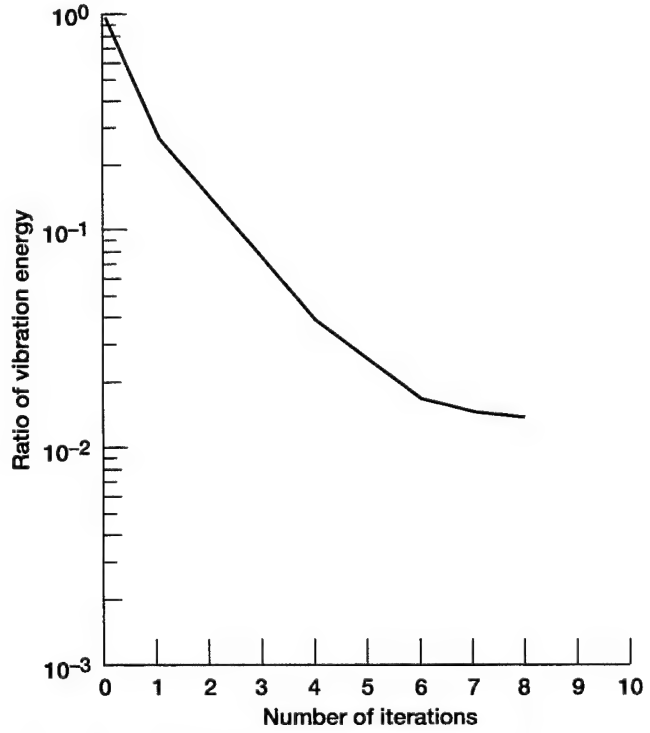


Figure 35.—Convergence of vibration energy by iteration number for optimization of simply supported plate. Excitation frequency $f_{ex}$ = 390 Hz.

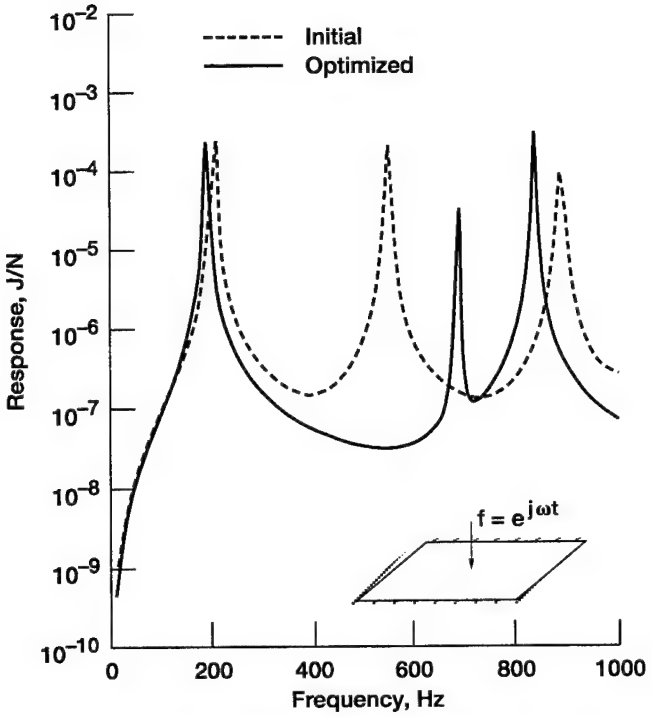


Figure 36.—Frequency response of clamped plate. Excitation frequency $f_{ex}$ = 530 Hz.

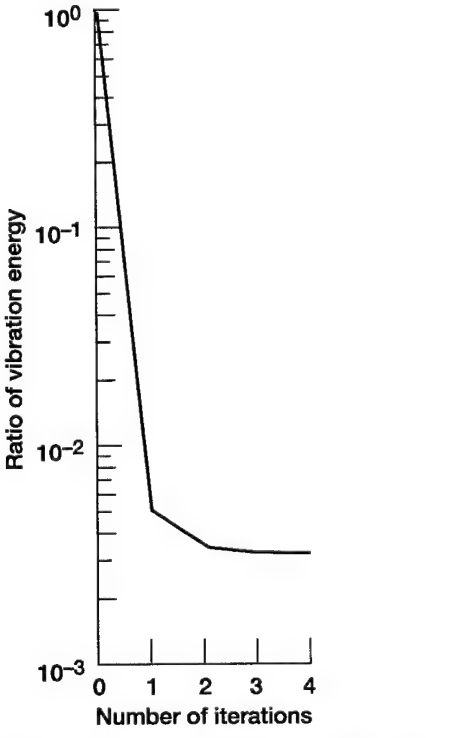


Figure 37.—Convergence of vibration energy by iteration number for optimization of clamped plate. Excitation frequency $f_{ex}$ = 530 Hz.

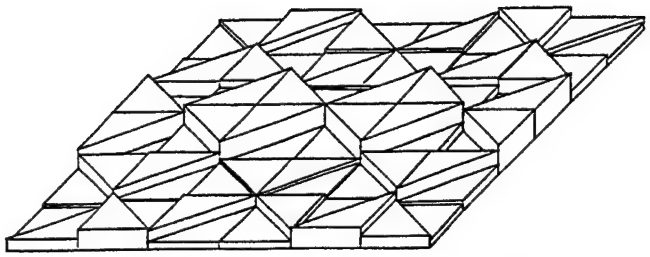

Figure 38.—Optimum shape of clamped plate. Excitation frequency $f_{ex}$ = 530 Hz.

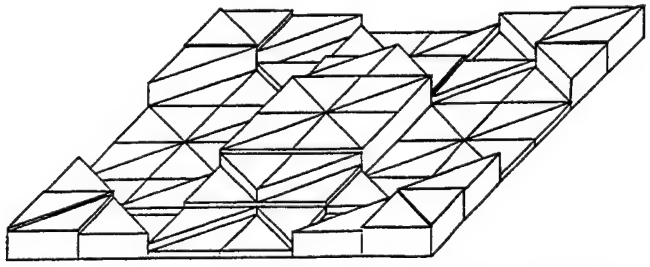

Figure 39.—Optimum shape of clamped plate. Excitation frequency $f_{ex}$ = 550 Hz.

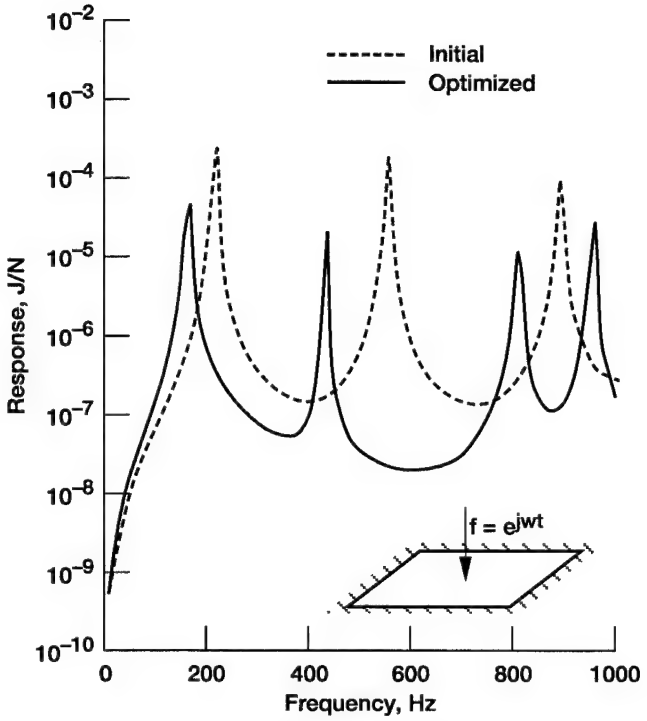


Figure 40.—Frequency response of clamped plate. Excitation frequency $f_{ex}$ = 550 Hz.

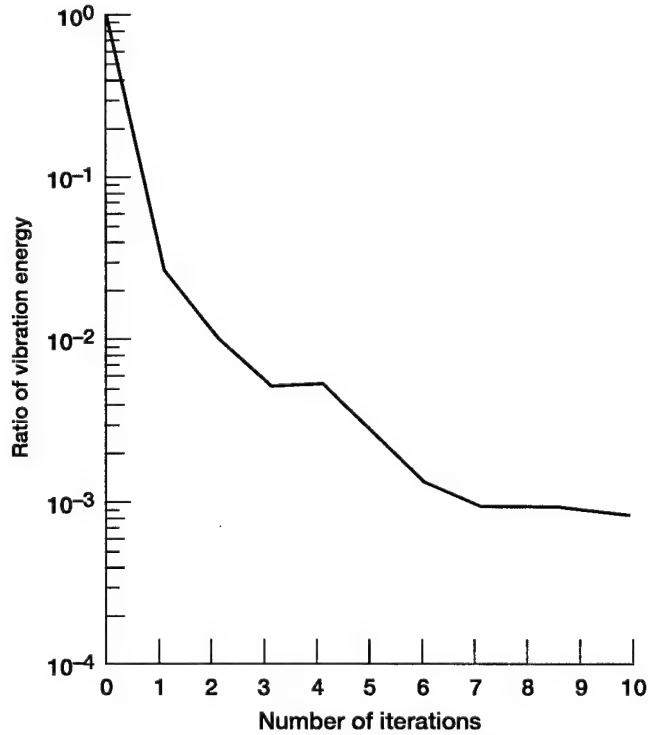


Figure 41.—Convergence of vibration energy by iteration number for optimization of clamped plate. Excitation frequency $f_{ex}$ = 550 Hz.

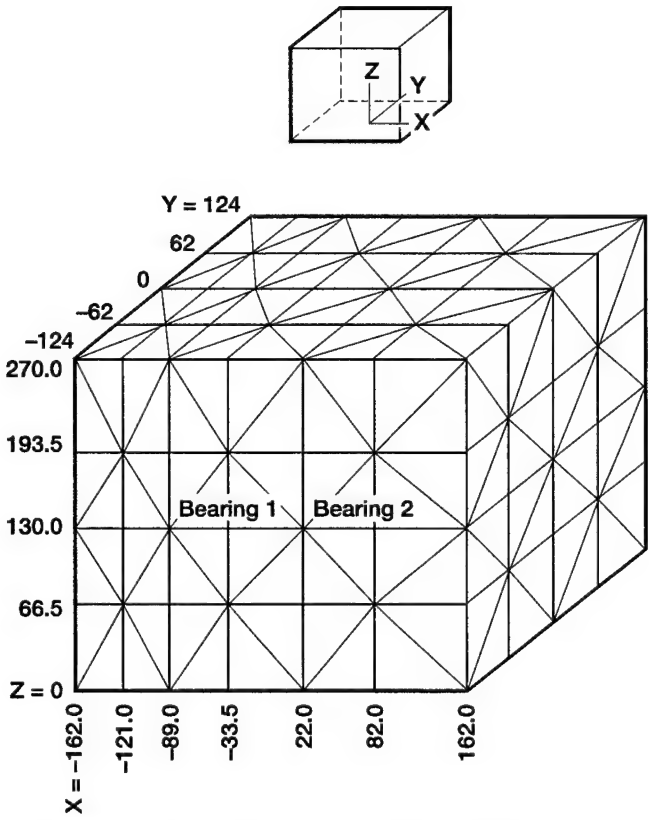


Figure 42.—Finite element mesh pattern used for the optimum design of NASA test gearbox.

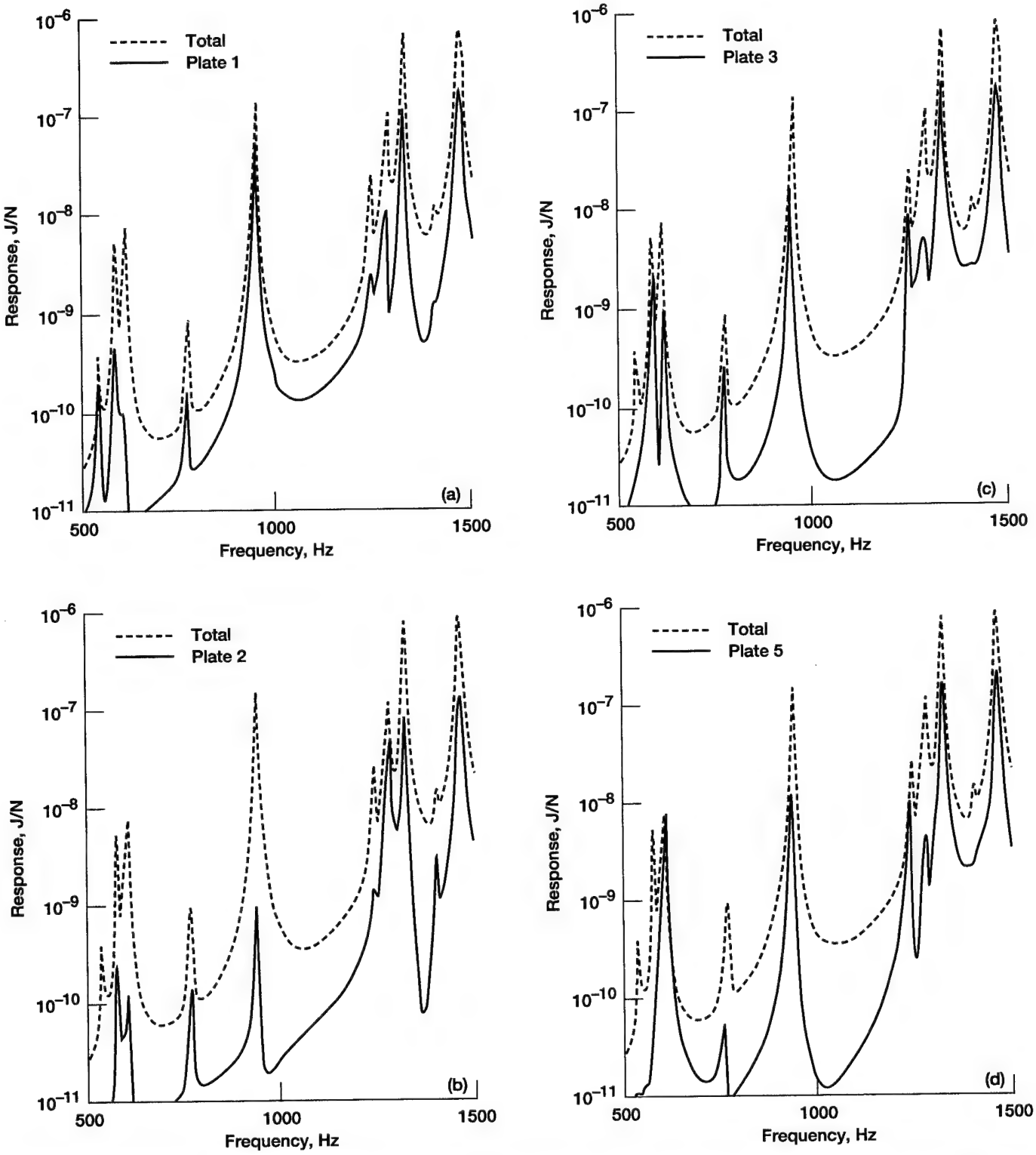


Figure 43.—Frequency response of NASA gearbox with initial thickness showing total vibration energy response and contribution of each plate to total. (a) Contribution of plate 1 (top) on vibration energy. (b) Contribution of plate 2 on vibration energy. (c) Contribution of plate 3 on vibration energy. (d) Contribution of plate 5 on vibration energy. (e) Contribution of plate 6 on vibration energy.

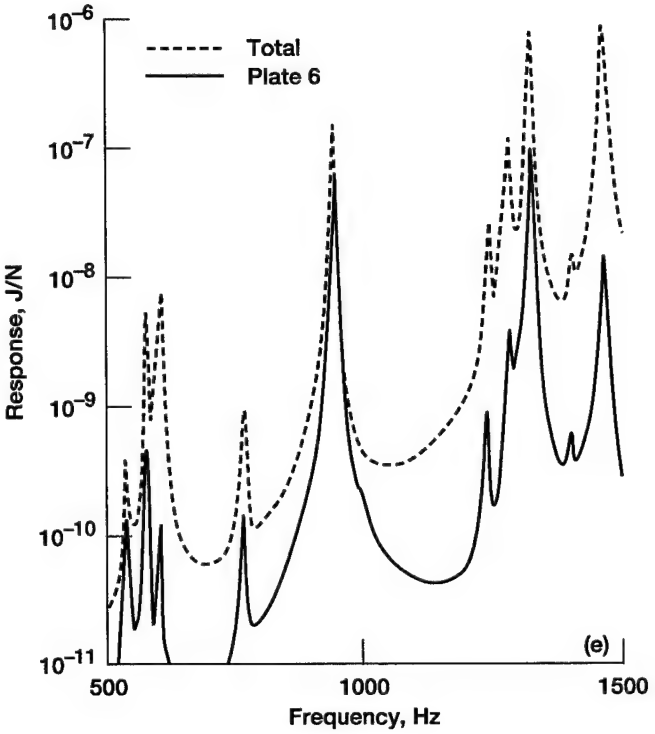


Figure 43.—Concluded. (e) Contribution of plate 6 on vibration energy.

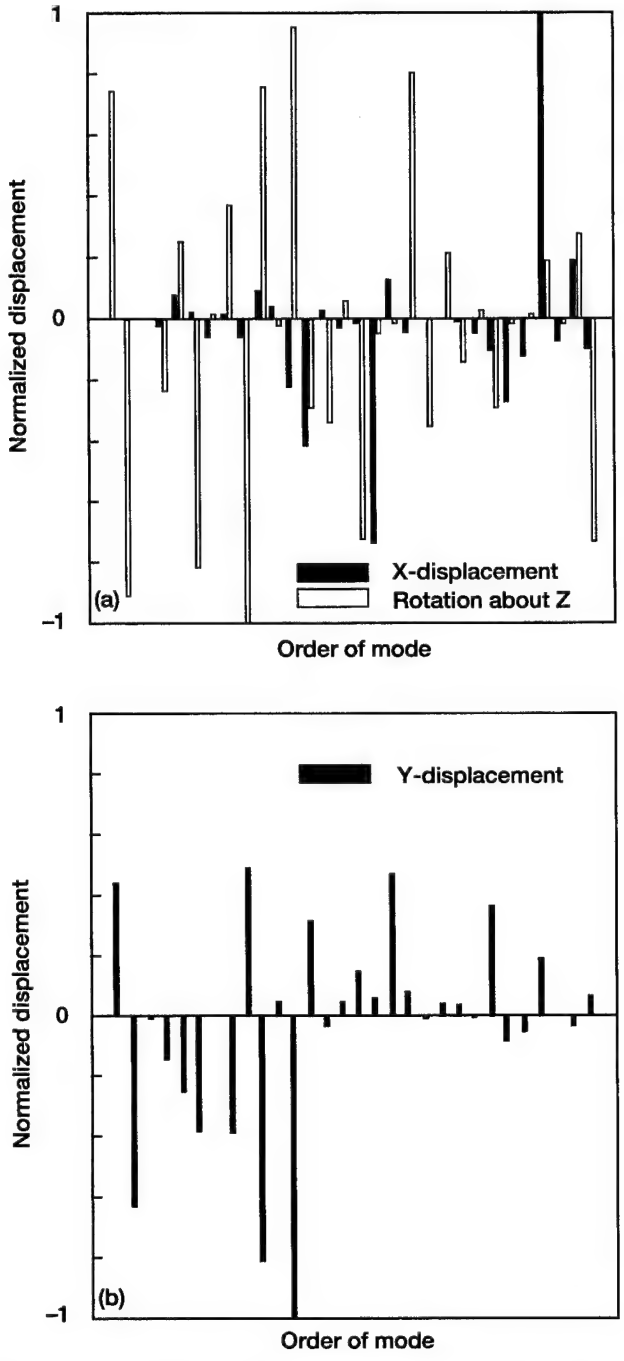


Figure 44.— Relative displacements at bearing location as function of mode order. (a) Displacement along X axis and rotation about Z axis for bearing 1. (b) Displacement along Y axis for bearing 1. (c) Displacement along Z axis and rotation about X axis for bearing 1. (d) Displacement along X axis and rotation about Z axis for bearing 2. (e) Displacement along Y axis for bearing 2. (f) Displacement along Z axis and rotation about X axis for bearing 2.

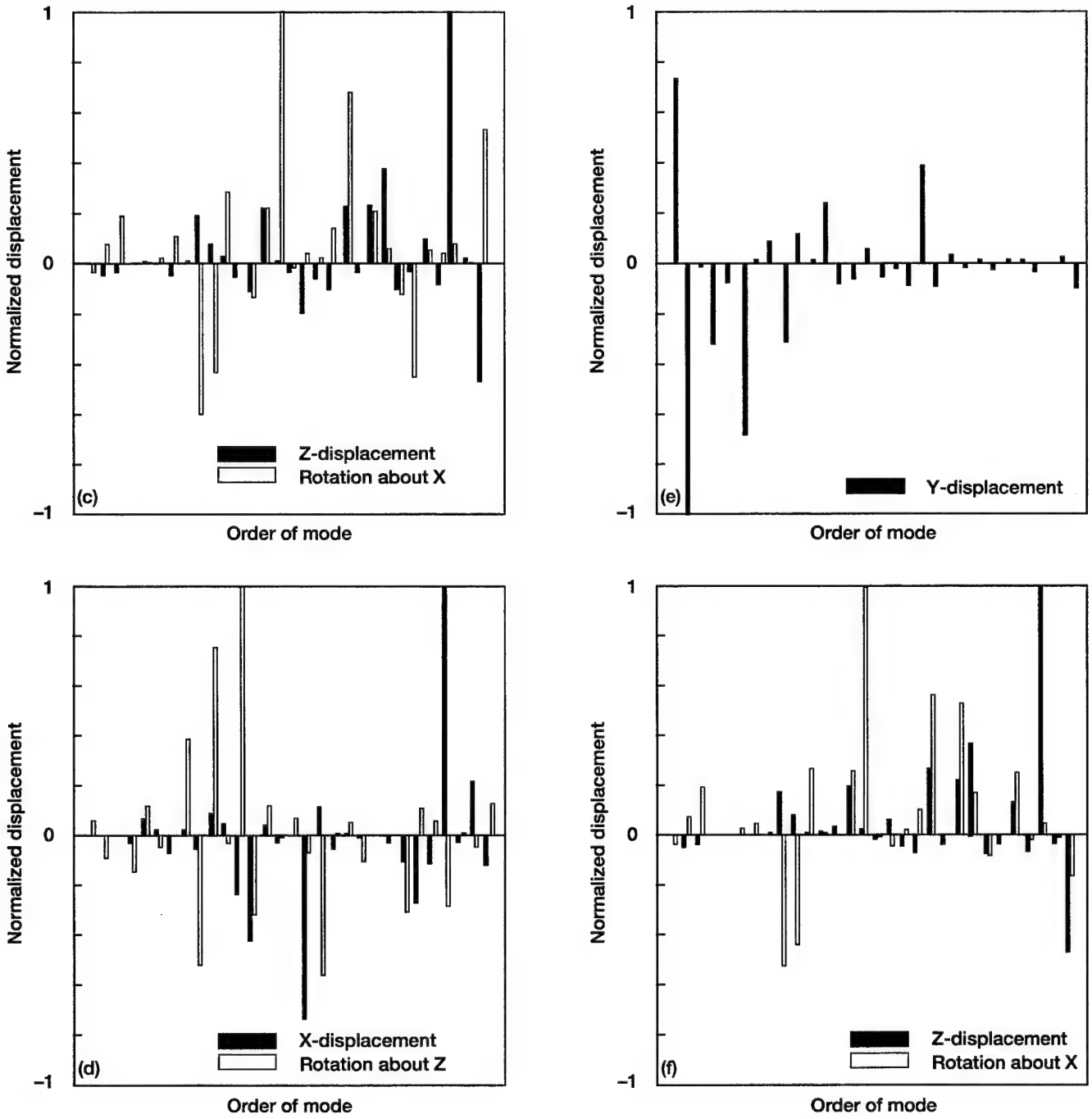


Figure 44.— Concluded. (c) Displacement along Z axis and rotation about X axis for bearing 1. (d) Displacement along X axis and rotation about Z axis for bearing 2. (e) Displacement along Y axis for bearing 2. (f) Displacement along Z axis and rotation about X axis for bearing 2.

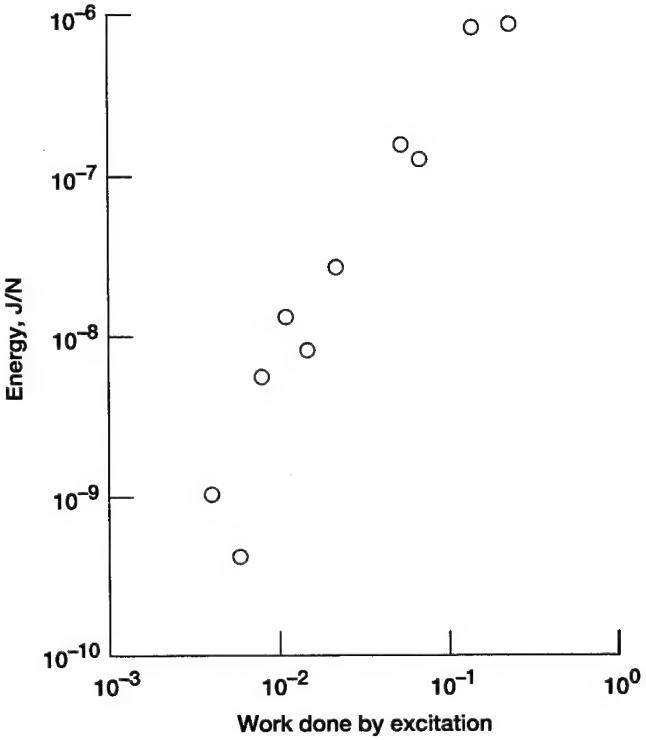


Figure 45.—Relation between vibration energy of gearbox and relative work done by exciting force.

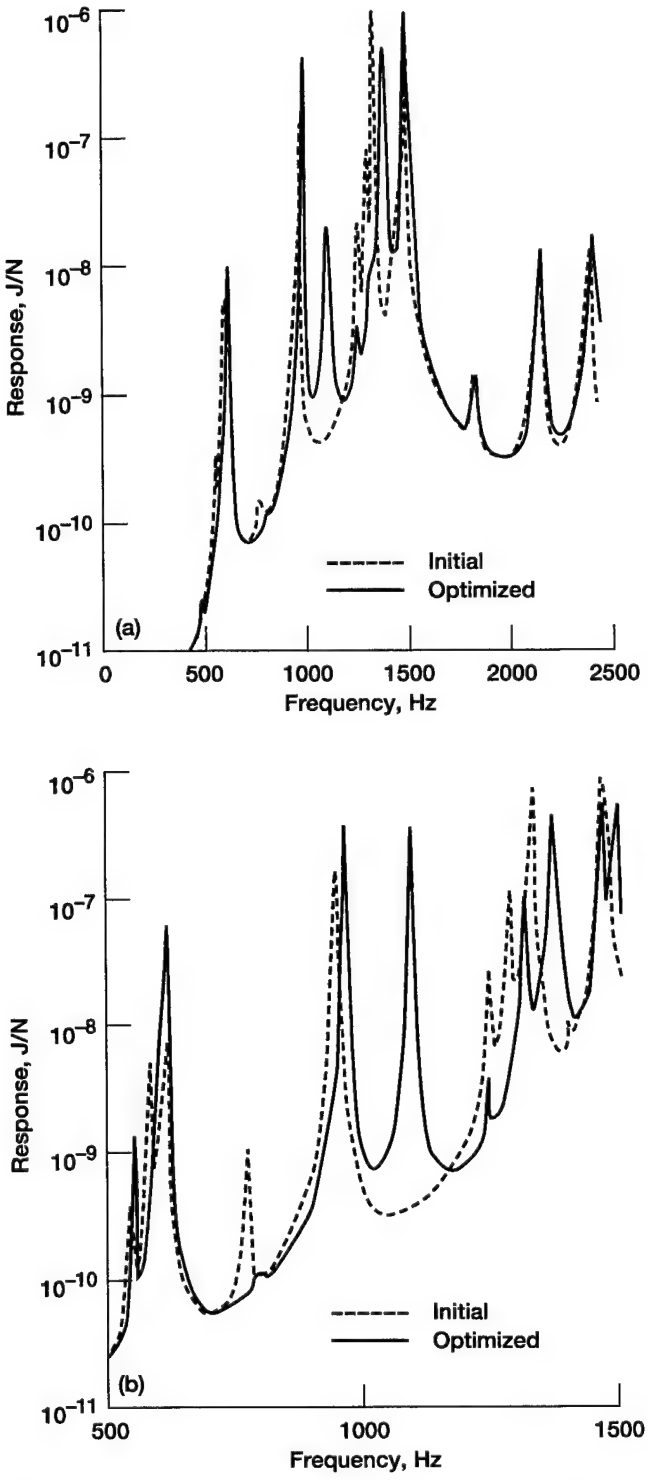


Figure 46.—Frequency response of NASA gearbox with shape of top plate optimized for minimum vibration energy.
(a) Response in frequency range 400 through 2400 Hz.
(b) Response in frequency range 500 through 1500 Hz.

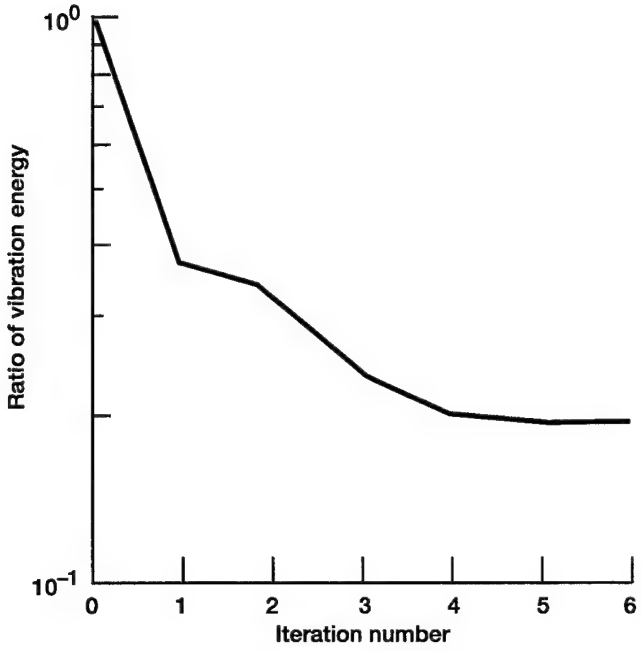


Figure 47.—Convergence of vibration energy by iteration number for optimization of NASA test gearbox top plate only.

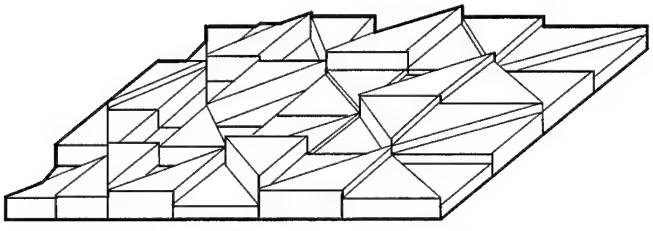

Figure 48.—Optimum shape of NASA test gearbox top plate for minimum vibration energy when optimizing top-plate shape only.

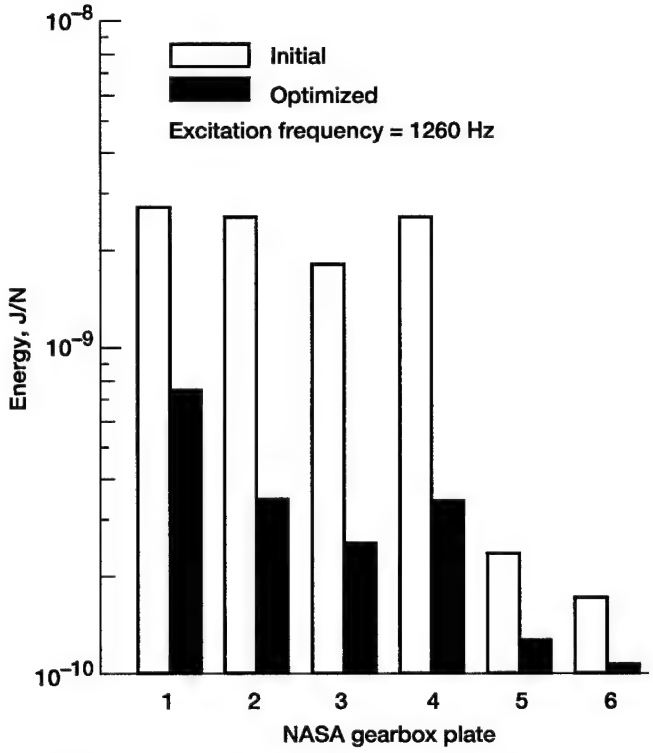


Figure 49.—Vibration energy response of each NASA test gearbox plate for initial design and after optimizing top-plate.

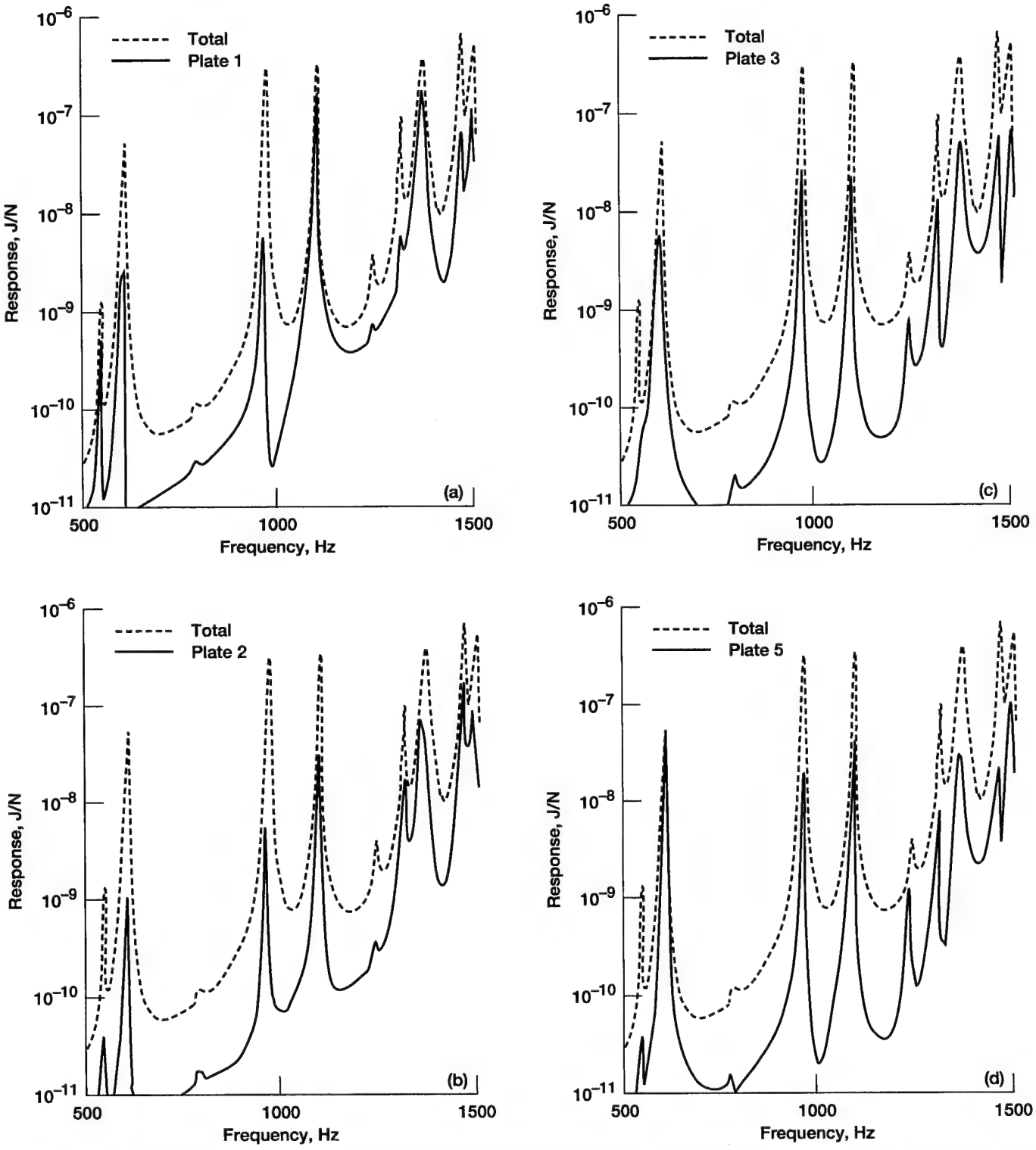


Figure 50.—Frequency response of NASA gearbox with top plate optimized only. (a) Plate 1 (top). (b) Plate 2. (c) Plate 3. (d) Plate 5. (e) Plate 6.

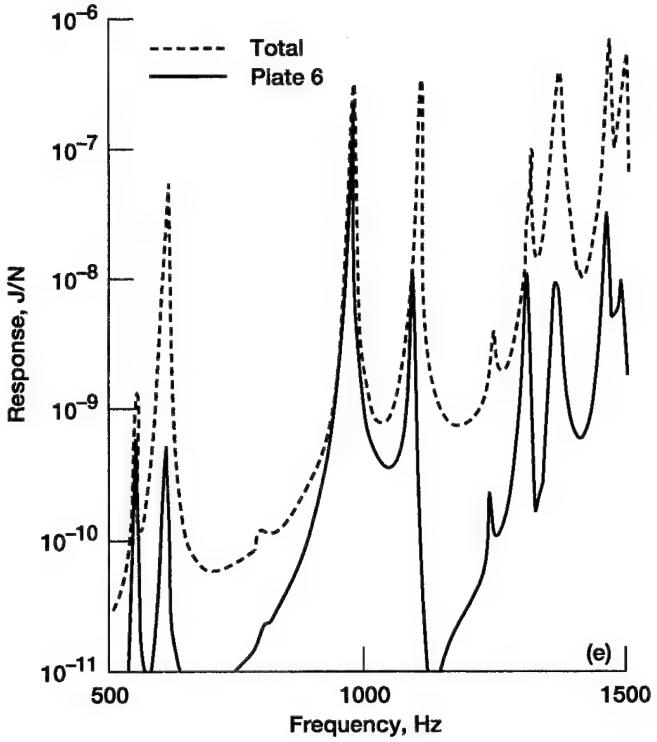


Figure 50.—Concluded. (e) Plate 6.

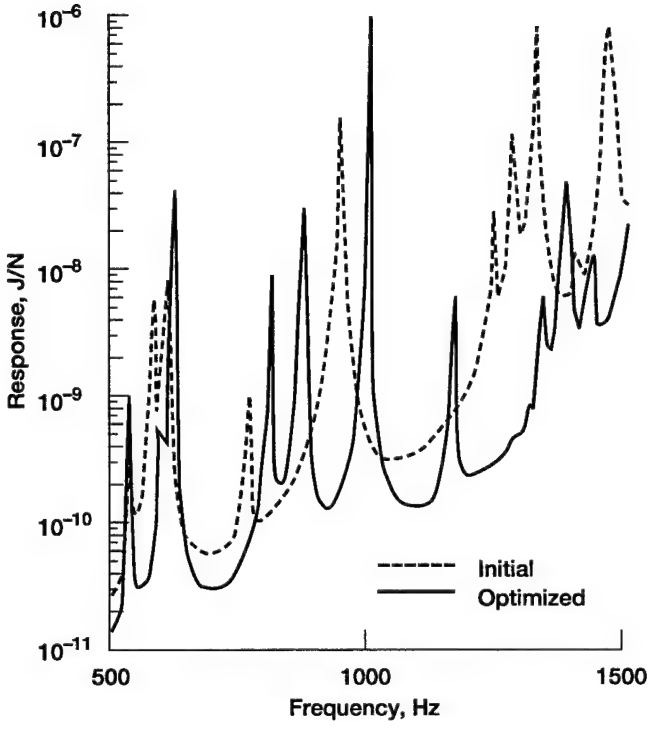


Figure 51.—Frequency response of NASA gearbox with shape of top and two side plates optimized for minimum vibration energy.

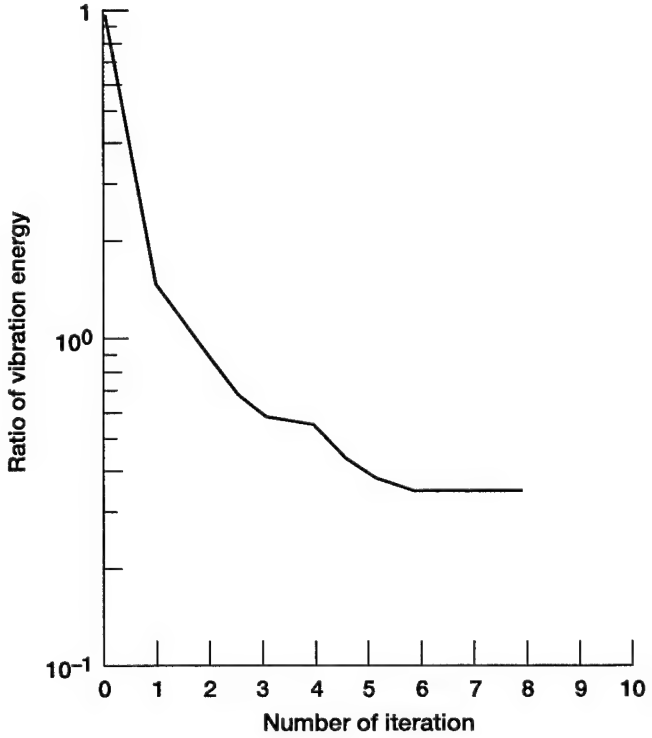


Figure 52—Convergence of vibration energy by iteration number for optimization of NASA test gearbox top and two side plates.

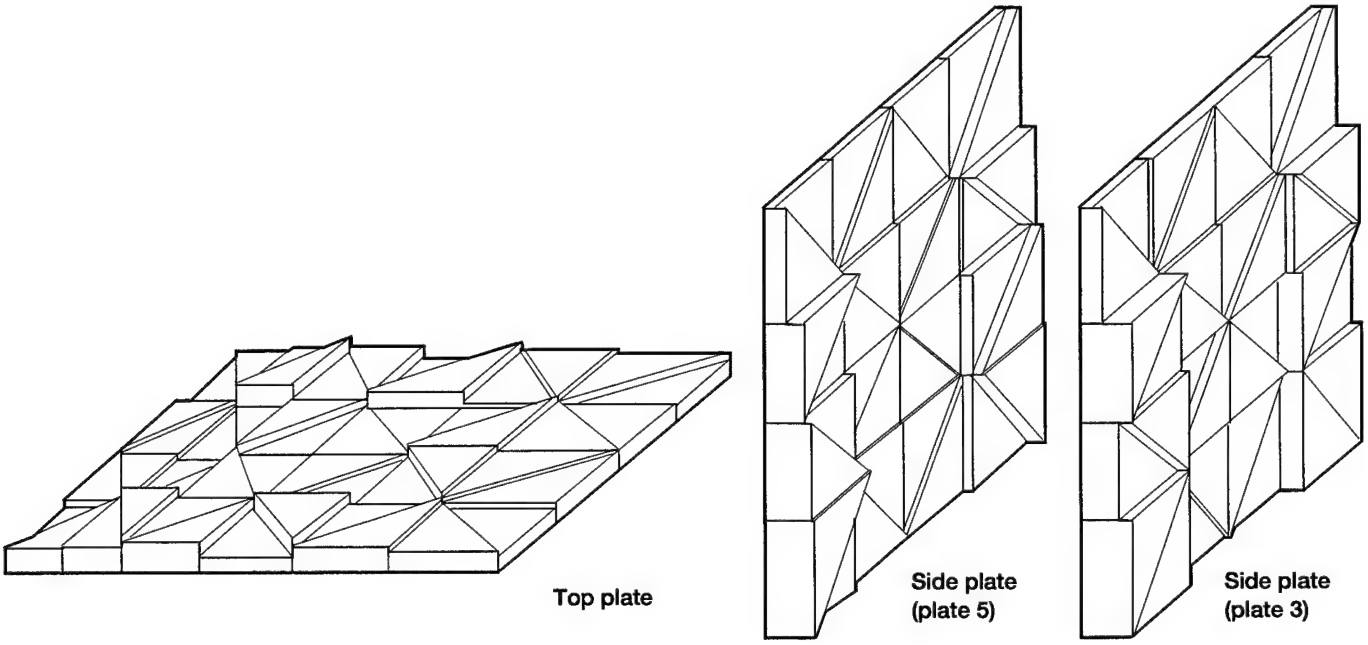


Figure 53.—Optimum shape of NASA test gearbox top and two side plates for minimum vibration energy when optimizing all three sides simultaneously.

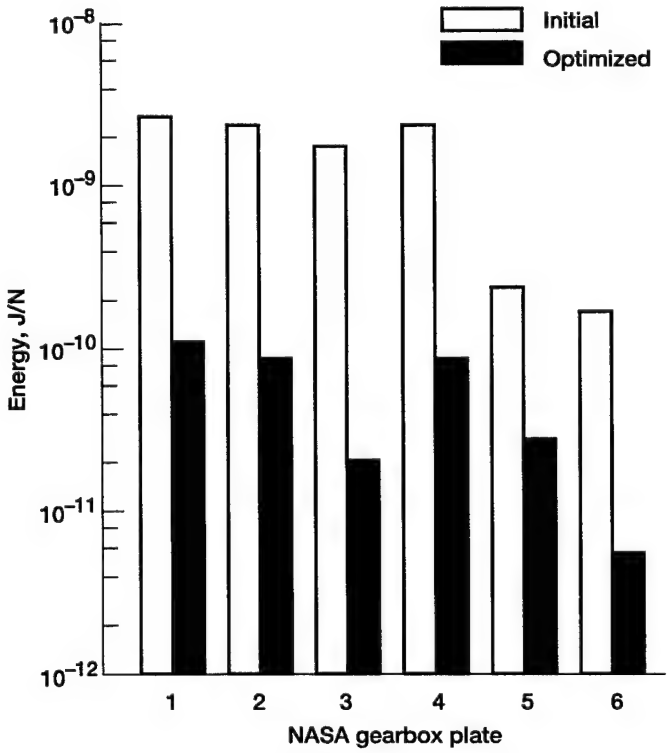


Figure 54.—Vibration energy response of each NASA test gearbox plate for initial design and after optimizing top (plate 1) and sides (plates 3 and 5) simultaneously.

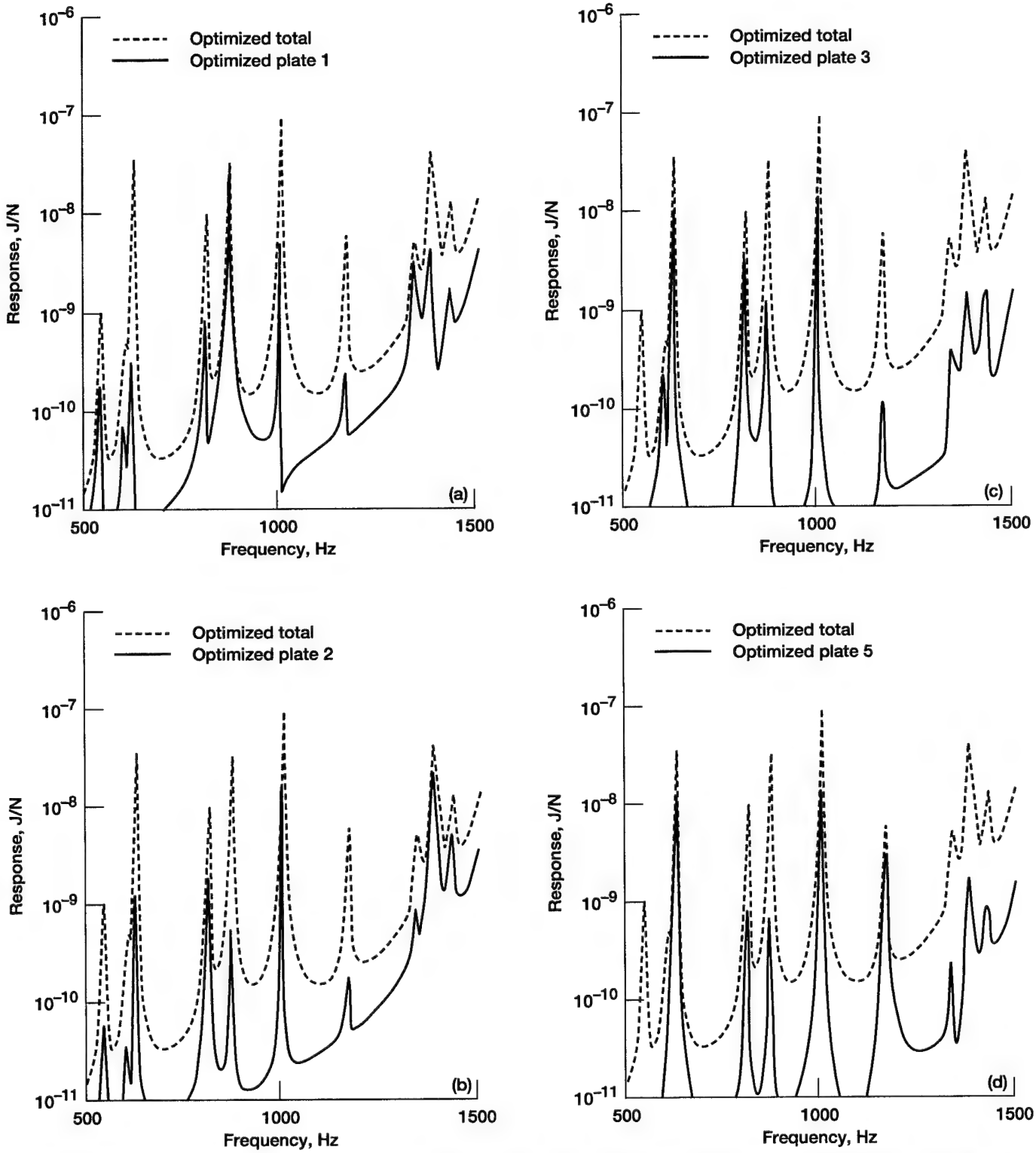


Figure 55.—Frequency response of each NASA gearbox plate with shapes of top (plate 1) and sides (plates 3 and 5) optimized simultaneously for minimum vibration energy compared to total response. (a) Plate 1 (top). (b) Plate 2. (c) Plate 3. (d) Plate 5. (e) Plate 6.

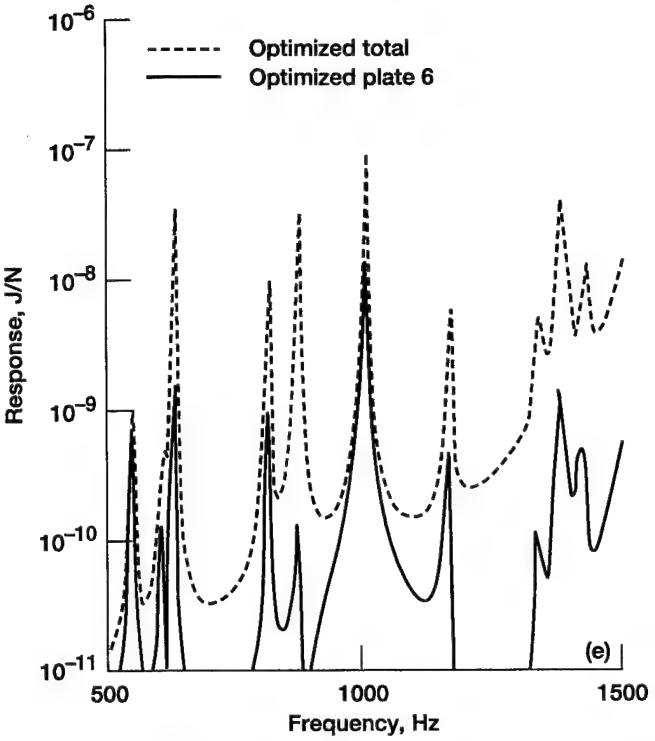


Figure 55.—Concluded. (e) Plate 6.

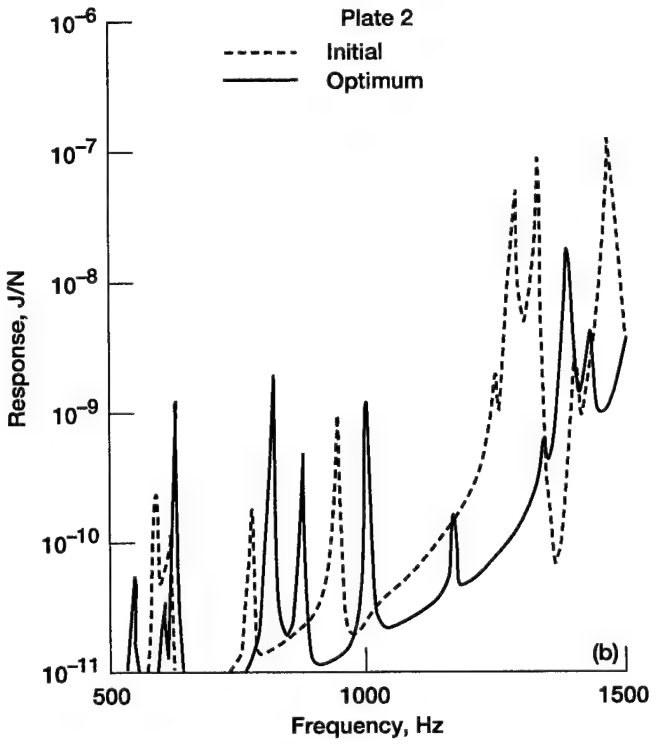


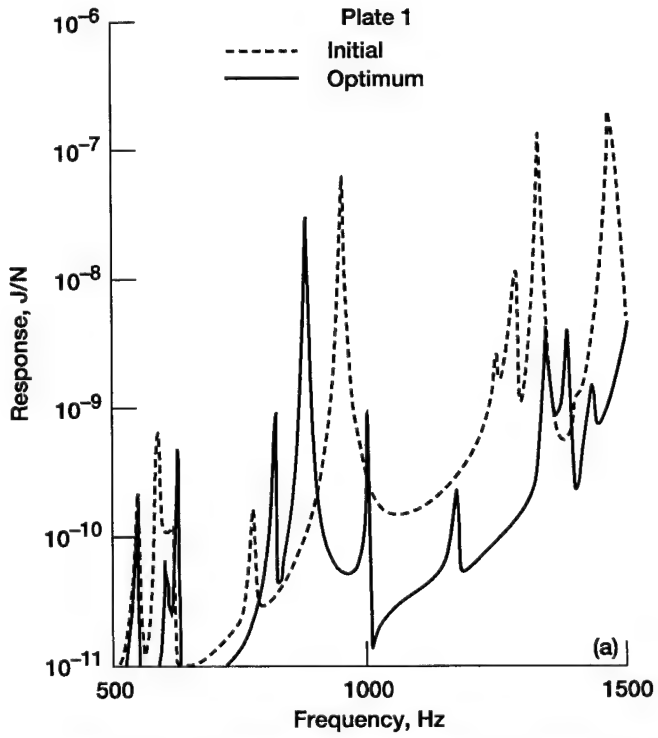


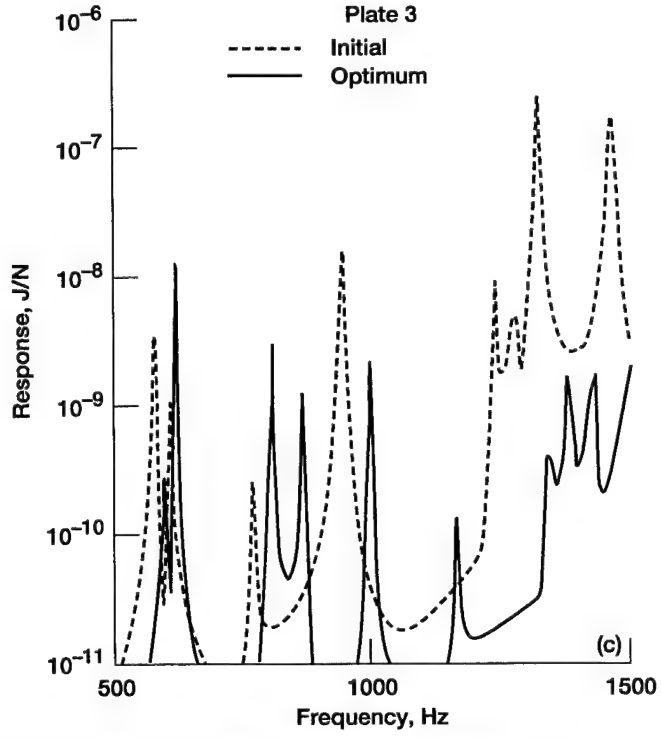


Figure 56.—Frequency response of each plate before and after optimization for case of optimizing top (plate 1) and sides (plates 3 and 5) simultaneously for minimum vibration energy. (a) Plate 1 (top). (b) Plate 2. (c) Plate 3 (side). (d) Plate 5 (side). (e) Plate 6.

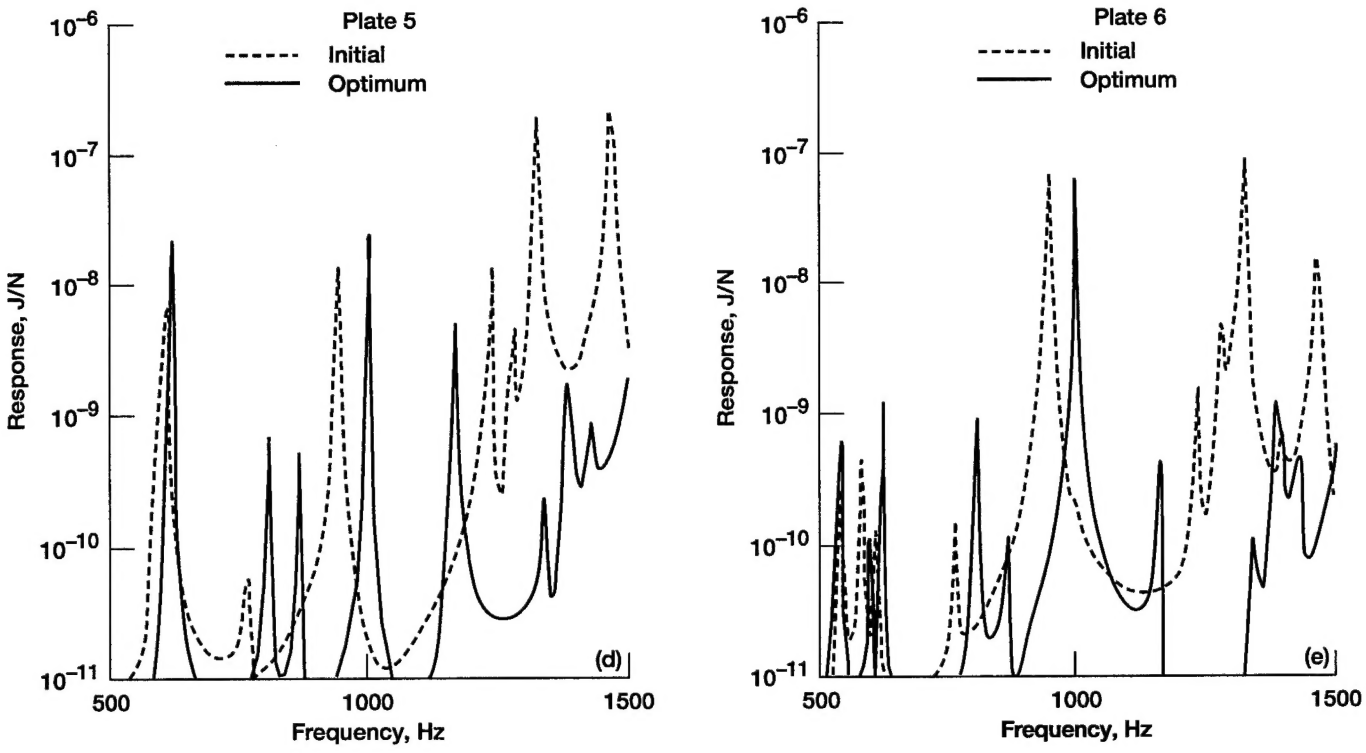


Figure 56.—Concluded. (d) Plate 5 (side). (e) Plate 6.

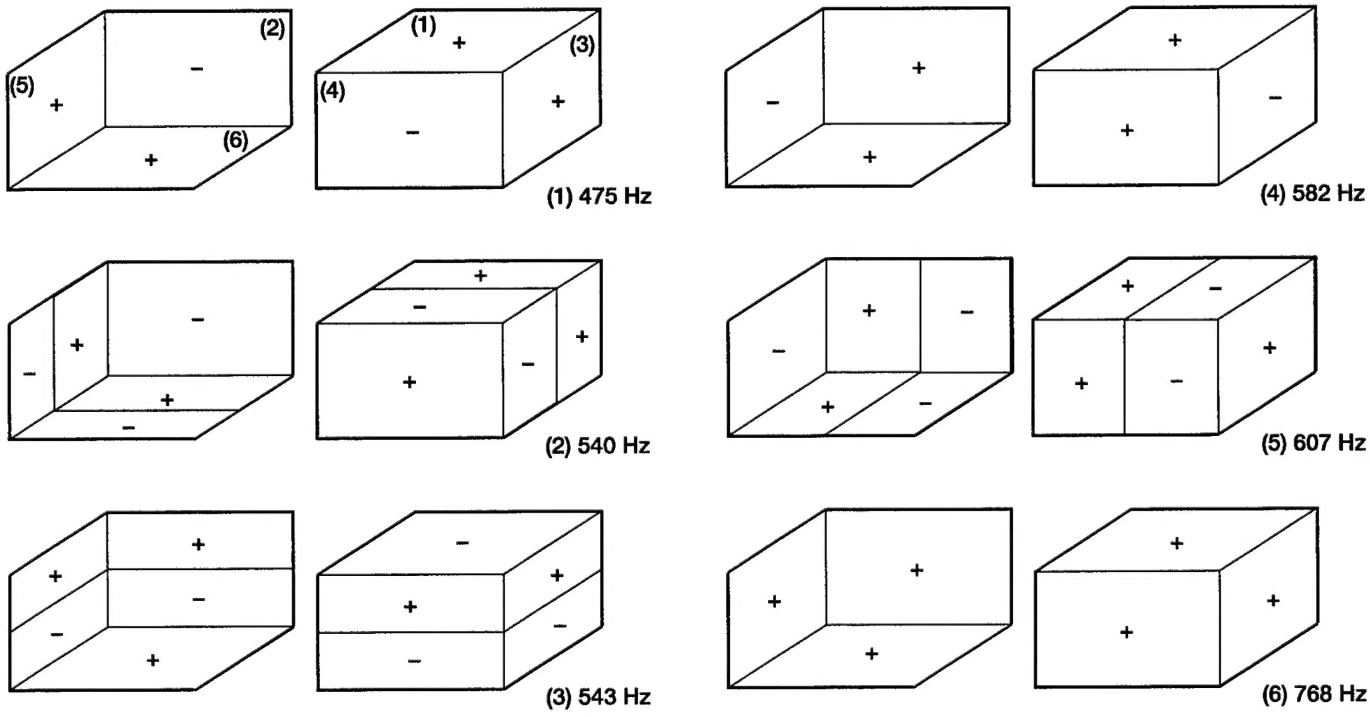


Figure 57.—NASA test gearbox computed mode shapes.

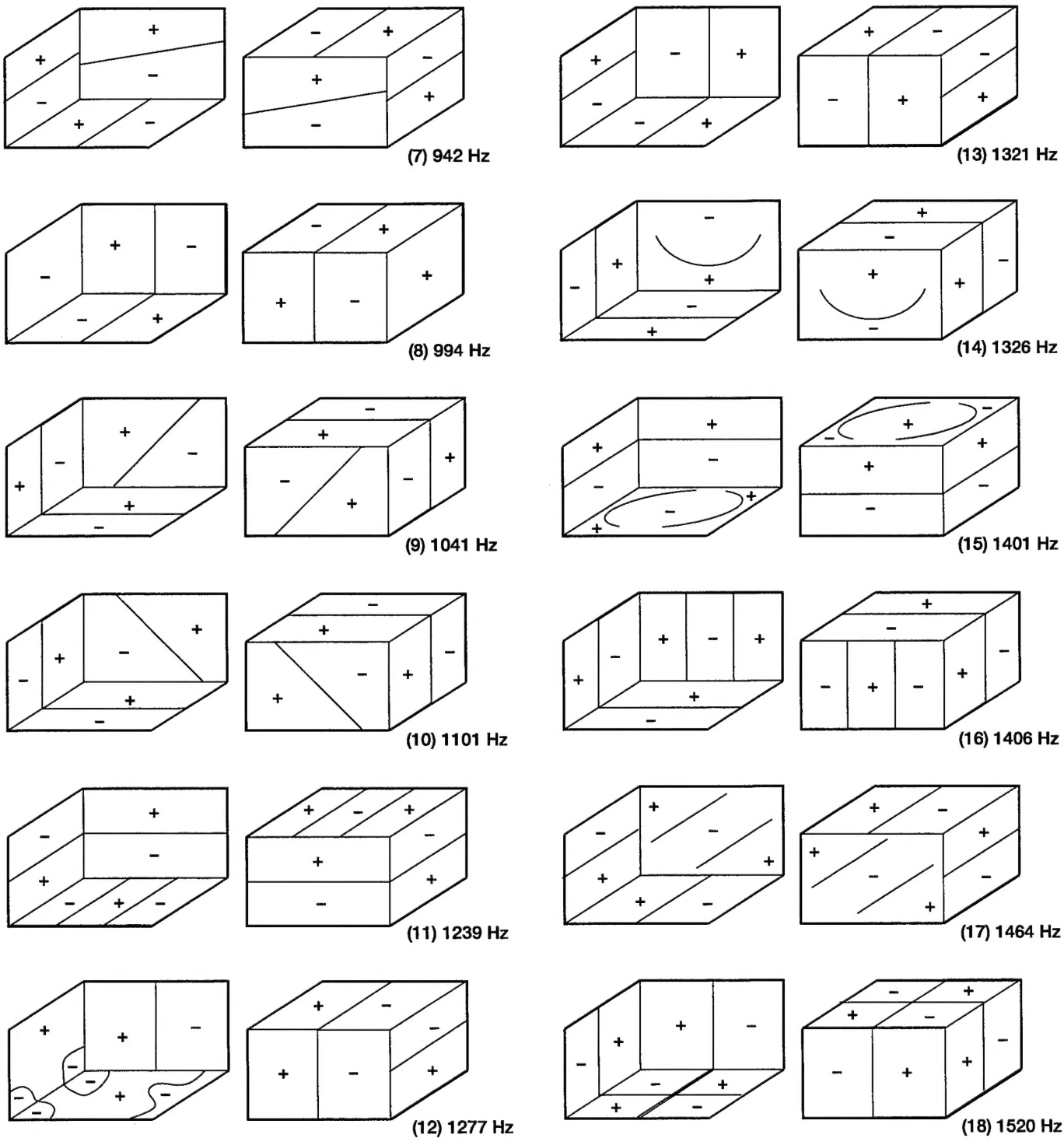


Figure 57.—Continued.

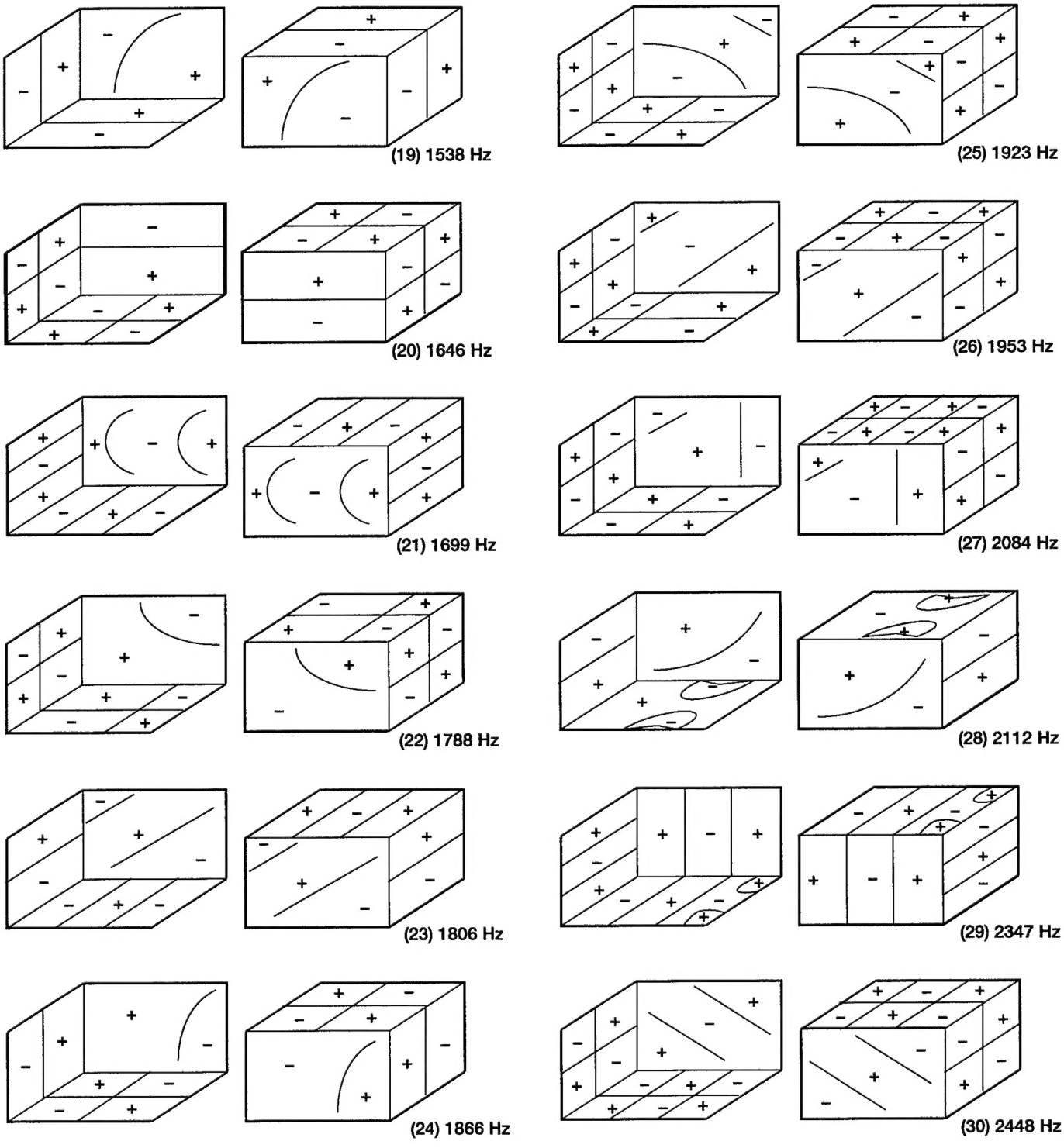


Figure 57.—Concluded.

# REPORT DOCUMENTATION PAGE

*Form Approved*
*OMB No. 0704-0188*



| 1. AGENCY USE ONLY (*Leave blank*) | 2. REPORT DATE | 3. REPORT TYPE AND DATES COVERED |
|---|---|---|
| | December 1995 | Technical Memorandum |

**4. TITLE AND SUBTITLE**

Minimization of the Vibration Energy of Thin-Plate Structures and the Application to the Reduction of Gearbox Vibration

**5. FUNDING NUMBERS**

WU–505–62–36
1L162211A47A

**6. AUTHOR(S)**

Katsumi Inoue and Timothy L. Krantz

**7. PERFORMING ORGANIZATION NAME(S) AND ADDRESS(ES)**

NASA Lewis Research Center
Cleveland, Ohio 44135–3191
and
Vehicle Propulsion Directorate
U.S. Army Research Laboratory
Cleveland, Ohio 44135–3191

**8. PERFORMING ORGANIZATION REPORT NUMBER**

E–9505

**9. SPONSORING/MONITORING AGENCY NAME(S) AND ADDRESS(ES)**

National Aeronautics and Space Administration
Washington, D.C. 20546–0001
and
U.S. Army Research Laboratory
Adelphi, Maryland 20783–1145

**10. SPONSORING/MONITORING AGENCY REPORT NUMBER**

NASA TM–106878
ARL–TR–722

**11. SUPPLEMENTARY NOTES**

Katsumi Inoue, National Research Council—NASA Research Associate at Lewis Research Center (presently at Tohoku University, Sendai, Japan), and Timothy L. Krantz, Vehicle Propulsion Directorate, U.S. Army Research Laboratory, NASA Lewis Research Center. Responsible person, Timothy L. Krantz, organization code 2730, (216) 433–3580.

**12a. DISTRIBUTION/AVAILABILITY STATEMENT**

Unclassified - Unlimited
Subject Category 37

This publication is available from the NASA Center for Aerospace Information, (301) 621–0390.

**12b. DISTRIBUTION CODE**

**13. ABSTRACT** (*Maximum 200 words*)

While the vibration analysis of gear systems has been developed, a systematic approach to the reduction of gearbox vibration has been lacking. The technique of reducing vibration by shifting natural frequencies is proposed here for gearboxes and other thin-plate structures using the theories of finite elements, modal analysis, and optimization. A triangular shell element with 18 degrees of freedom is developed for structural and dynamic analysis. To optimize, the overall vibration energy is adopted as the objective function to be minimized at the excitation frequency by varying the design variable (element thickness) under the constraint of overall constant weight. Modal analysis is used to determine the sensitivity of the vibration energy as a function of the eigenvalues and eigenvectors. The optimum design is found by the gradient projection method and a unidimensional search procedure. By applying the computer code to design problems for beams and plates, it was verified that the proposed method is effective in reducing vibration energy. The computer code is also applied to redesign the NASA Lewis gear noise rig test gearbox housing. As one example, only the shape of the top plate is varied, and the vibration energy levels of all the surfaces are reduced, yielding an overall reduction of 1/5 compared to the initial design. As a second example, the shapes of the top and two side plates are varied to yield an overall reduction in vibration energy of 1/30.

**14. SUBJECT TERMS**

Gearbox; Vibration; Optimization; Finite element method; Modal analysis

**15. NUMBER OF PAGES**

50

**16. PRICE CODE**

A03

| 17. SECURITY CLASSIFICATION OF REPORT | 18. SECURITY CLASSIFICATION OF THIS PAGE | 19. SECURITY CLASSIFICATION OF ABSTRACT | 20. LIMITATION OF ABSTRACT |
|---|---|---|---|
| Unclassified | Unclassified | Unclassified | |